Author/s:
Ganley, M;Holz, LE;Minnell, JJ;de Menezes, MN;Burn, OK;Poa, KCY;Draper, SL;English, K;Chan, STS;Anderson, RJ;Compton, BJ;Marshall, AJ;Cozijnsen, A;Chua, YC;Ge, Z;Farrand, KJ;Mamum, JC;Xu, C;Cockburn, IA;Yui, K;Bertolino, P;Gras, S;Le Nours, J;Rossjohn, J;Fernandez-Ruiz, D;McFadden, GI;Ackerley, DF;Painter, GF;Hermans, IF;Heath, WR

Title:
mRNA vaccine against malaria tailored for liver-resident memory T cells

Date:
2023-09-01

Citation:
Ganley, M., Holz, L. E., Minnell, J. J., de Menezes, M. N., Burn, O. K., Poa, K. C. Y., Draper, S. L., English, K., Chan, S. T. S., Anderson, R. J., Compton, B. J., Marshall, A. J., Cozijnsen, A., Chua, Y. C., Ge, Z., Farrand, K. J., Mamum, J. C., Xu, C., Cockburn, I. A. ,... Heath, W. R. (2023). mRNA vaccine against malaria tailored for liver-resident memory T cells. Nature Immunology, 24 (9), pp.1487-1498. https://doi.org/10.1038/s41590-023-01562-6.

nature immunology

Article

https://doi.org/10.1038/s41590-023-01562-6

mRNA vaccine against malaria tailored for liver-resident memory T cells

Received: 30 November 2022

Accepted: 15 June 2023

Published online: 20 July 2023

Check for updates

Mitch Ganley[1,2,13], Lauren E. Holz[3,13], Jordan J. Minnell[4], Maria N. de Menezes[3], Olivia K. Burn[4], Kean Chan Yew Poa[5], Sarah L. Draper[1], Kieran English[6], Susanna T. S. Chan[1], Regan J. Anderson[1], Benjamin J. Compton[1], Andrew J. Marshall[1], Anton Cozijnsen[7], Yu Cheng Chua[3], Zhengyu Ge[3], Kathryn J. Farrand[4], John C. Mamum[4], Calvin Xu[3], Ian A. Cockburn[8], Katsuyuki Yui[9], Patrick Bertolino[6], Stephanie Gras[5,10], Jérôme Le Nours[5], Jamie Rossjohn[5,11], Daniel Fernandez-Ruiz[3], Geoffrey I. McFadden[7], David F. Ackerley[2,12], Gavin F. Painter[1,2,14] ✉, Ian F. Hermans[2,4,14] ✉ & William R. Heath[3,14] ✉

Malaria is caused by *Plasmodium* species transmitted by *Anopheles* mosquitoes. Following a mosquito bite, *Plasmodium* sporozoites migrate from skin to liver, where extensive replication occurs, emerging later as merozoites that can infect red blood cells and cause symptoms of disease. As liver tissue-resident memory T cells (Trm cells) have recently been shown to control liver-stage infections, we embarked on a messenger RNA (mRNA)-based vaccine strategy to induce liver Trm cells to prevent malaria. Although a standard mRNA vaccine was unable to generate liver Trm or protect against challenge with *Plasmodium berghei* sporozoites in mice, addition of an agonist that recruits T cell help from type I natural killer T cells under mRNA-vaccination conditions resulted in significant generation of liver Trm cells and effective protection. Moreover, whereas previous exposure of mice to blood-stage infection impaired traditional vaccines based on attenuated sporozoites, mRNA vaccination was unaffected, underlining the potential for such a rational mRNA-based strategy in malaria-endemic regions.

With the advent of the COVID-19 pandemic, vaccines based on mRNA have had a major impact on human death and suffering. By contrast, the contribution of malaria to human morbidity and mortality has increased, and various intervention strategies for malaria have been negatively affected by the pandemic[1]. Development of a highly effective malaria vaccine remains a major goal.

Malaria is caused by a variety of *Plasmodium* species, with several capable of infecting humans[2]. There were 241 million cases of malaria in 2020 and over 627,000 associated deaths, the majority of which were caused by *Plasmodium falciparum* infection of children under 5 years old[1]. *Plasmodium* species have a complex lifecycle that includes a sexual stage of replication in mosquitos and two asexual stages in vertebrates[2]. Once introduced into the skin by mosquito bite, sporozoites make their way to the liver, where they infect and replicate extensively in hepatocytes. This stage is asymptomatic in humans; however, within about 1 week, merozoites are released into the blood, where they cause cyclic reinfection of red blood cells (RBC) and all symptoms of disease.

Although morbidity and mortality associated with malaria have been reduced significantly in the past two decades, largely through interventions that control mosquitos or by administration of drugs that limit human infection, these interventions have been disrupted by the COVID-19 pandemic, resulting in recent increases in disease and death[1]. Even without the devastating effects of the pandemic, drug resistance in parasites and insecticide resistance in mosquitos necessitate development of an effective malaria vaccine[3].

A full list of affiliations appears at the end of the paper. ✉e-mail: gavin.painter@vuw.ac.nz; ihermans@malaghan.org.nz; wrheath@unimelb.edu.au

Malaria vaccination strategies can be grouped by the parasite life-cycle stage they target. For vaccines targeting migrating sporozoites or blood-stage infection, antibodies have been the primary effector mechanism. Several vaccination approaches have been used to induce antibodies against sporozoite surface proteins to impair parasites before they infect hepatocytes. This is the basis of the first licensed malaria vaccine, RTS,S, which has been broadly approved for human use but is only moderately effective[4]. The limited efficacy of RTS,S is in part due to the very short time window available for antibodies to impair sporozoites during their migration to the liver; however, there are also effects of antigen polymorphism and suboptimal vaccine design[5]. A newer related vaccine, R21, appears to offer superior efficacy but is at an earlier stage of assessment[6,7]. Vaccines against blood-stage antigens have been extensively examined and are being developed but have been hampered by issues including antigen polymorphism and redundant invasion pathways[5]. The third major vaccination strategy involves generation of CD8 T cell immunity capable of killing infected hepatocytes, thereby preventing the parasite egress that results in blood-stage infection and associated disease. Subunit vaccines against antigens expressed during the liver stage have shown some efficacy but have again been limited by antigen polymorphism; they are also hampered by their probable failure to generate the most effective form of CD8 T cell immunity, that is, liver tissue-resident memory[8]. One approach that has been highly effective experimentally is the use of attenuated sporozoites that cannot progress to an infectious blood stage (the sporozoites are attenuated by irradiation, gene modifications or drug administration)[9,10]. When injected intravenously (i.v.), attenuated sporozoites induce efficient protection that is largely mediated by memory CD8 T cells[11]. Although circulating memory CD8 T cells may contribute to this protection[12], liver CD8 Trm cells are the most important effector population[8,10,13]. These cells reside permanently in the liver, patrolling the liver sinusoids to assess for infection of underlying hepatocytes[8,14]. The crucial role of liver Trm cells has been demonstrated by loss of protection after Trm cell depletion of mice vaccinated with attenuated sporozoites[8]. Indirect evidence also supports a major role for Trm cells in humans protected by vaccination with RAS[10]. Although this vaccination strategy has shown efficient protection of malaria-naive humans in clinical trials[15,16], its efficacy has been somewhat less promising in the field, particularly in the face of endemic infection[15,17–19]. Experimentally, this has been attributed in part to immunosuppression caused by preexposure to blood-stage infection, a potential barrier to vaccination[20].

Considering the prominent protective role of liver CD8 Trm cells, we and others have developed prime-and-trap[8,21] and prime-and-target[22] vaccination strategies that favor liver CD8 Trm cell induction. More recently, we have used a glycolipid–peptide vaccination strategy[23] that recruits help from type I natural killer T (NKT) cells, an innate-like T cell population that is enriched in the liver and found in various other lymphoid and nonlymphoid tissues[24], to generate large numbers of liver CD8 Trm cells. These strategies induce effective protection against liver-stage malaria but are limited by their complexity or their peptide-epitope dependence. Peptide-based vaccination approaches require knowledge of, and the ability to combine, sufficient human leukocyte antigen (HLA)-restricted epitopes to ensure population coverage. Currently, the relatively limited knowledge in this area[25], together with the prominent polymorphism of malaria antigens, makes this strategy difficult to implement. By contrast, mRNA-based vaccines enable whole-gene (and protein) expression, potentially providing a wealth of epitopes capable of greater population coverage. Given the rapid advancement and translation of mRNA-based vaccines in response to COVID-19, we aimed to develop a protective malaria vaccine, using conserved genes, for generation of liver Trm cells.

Here, we show that although mRNA vaccination can induce circulating memory CD8 T cells (effector memory (Tem) and central memory (Tcm) cells), it is relatively inefficient at inducing liver Trm cells or protecting against malaria. However, this deficiency can be overcome by addition of an NKT cell agonist. The prototypical NKT cell agonist α-galactosylceramide (αGC), also known as KRN7000 (ref. 26), was a relatively poor adjuvant for liver Trm cell induction; however, chemical modifications to this molecule yielded efficient responses and sterile protection against sporozoite challenge. Furthermore, whereas previous exposure to blood-stage infection impaired vaccination with attenuated sporozoites, mRNA vaccination was unaffected by this pretreatment, indicating that the mRNA approach may be more effective in malaria-endemic regions.

Results

Trm cell induction requires adjuvant

To test whether mRNA vaccines could induce CD8 Trm cells in the liver, mRNA encoding the model antigen chicken ovalbumin (OVA) was complexed in liposomes to form a lipoplex mRNA vaccine (see Methods for preparation); this was then used to vaccinate mice i.v., a route shown to favor the induction of this T cell subset[9]. To efficiently monitor immunity, initial experiments used CD45.2 C57BL/6 (B6) mice that had undergone adoptive transfer of CD45.1-expressing CD8 T cells from the OVA-specific TCR transgenic mouse, OT-I (Fig. 1a)[27]. Seven days after vaccination, analysis of blood from mice immunized with the standard OVA mRNA (mOVA) vaccine revealed a robust increase in OT-I cells (Fig. 1b, middle group), indicating immunogenicity. However, analysis of memory subpopulations from the liver (Fig. 1c–f) and spleen (Fig. 1g–i) on day 30 showed that mOVA alone induced circulating T cells (Tem and Tcm) but very few liver Trm cells. As our previous studies using a glycolipid–peptide conjugate vaccine had shown that help from type I NKT cells enables efficient liver Trm cell formation[23], we tested whether incorporating an active fluorescent derivative of αGC, BODIPY-αGC (αGC_B)[28], into our mRNA vaccine might improve this response. Whereas relatively similar responses were seen with this adjuvanted vaccine on day 7 in the blood (Fig. 1b, right group), greatly enhanced memory T cell responses were seen on day 30 (Fig. 1d–i), with a strong shift toward generation of Trm cells in the liver (Fig. 1e,f). Challenge of these B6 mice with OVA-expressing *P. berghei* ANKA (PbA) sporozoites, which infect the liver, showed that nearly all mice were protected from development of blood-stage infection when given a single dose of mRNA vaccine, provided the vaccine contained the NKT cell agonist (Fig. 1j). In this model, such sterile protection is extremely difficult to achieve, but a reduction in parasitemia on day 7 can be used to measure more subtle parasite killing in the liver. Here, there was no evidence of significant parasite killing unless the mRNA vaccine was adjuvanted by the NKT cell agonist αGC_B (Fig. 1k). Together, these data suggest that NKT cell-mediated help is required for mRNA vaccination to promote protective liver Trm cell formation .

Modification of αGC increases numbers of liver Trm cells

As our initial preparation of adjuvanted vaccine incorporated αGC_B, we investigated whether αGC itself was able to act as a Trm-inducing adjuvant. We therefore compared memory T cell responses in the liver after vaccination with mRNA vaccines containing either αGC or αGC_B in mice that had undergone adoptive transfer of $CD45.1^+$ OT-I cells (Fig. 2a,b). This showed that αGC_B was vastly superior to αGC with respect to its capacity to induce liver Trm cells. This outcome prompted further investigation of alternative modifications to αGC and their effects on its adjuvant activity (Fig. 2c). As αGC_B differed by the addition of a large fluorescent BODIPY moiety that was attached via a thiol installed at the 6-position of the galactose, we tested a simpler structure that included the introduced 6-thiol without further modification (αGC_S)[29] and another that had an amino group installed at this position (αGC_N)[30] (Fig. 2c). Either of these simple modifications to the galactosyl-ring primary hydroxyl of αGC enhanced the capacity of mRNA to induce liver Trm cells (Fig. 2b). This coincided with an improved capacity to stimulate type I NKT cells resident in both the liver

https://doi.org/10.1038/s41590-023-01562-6

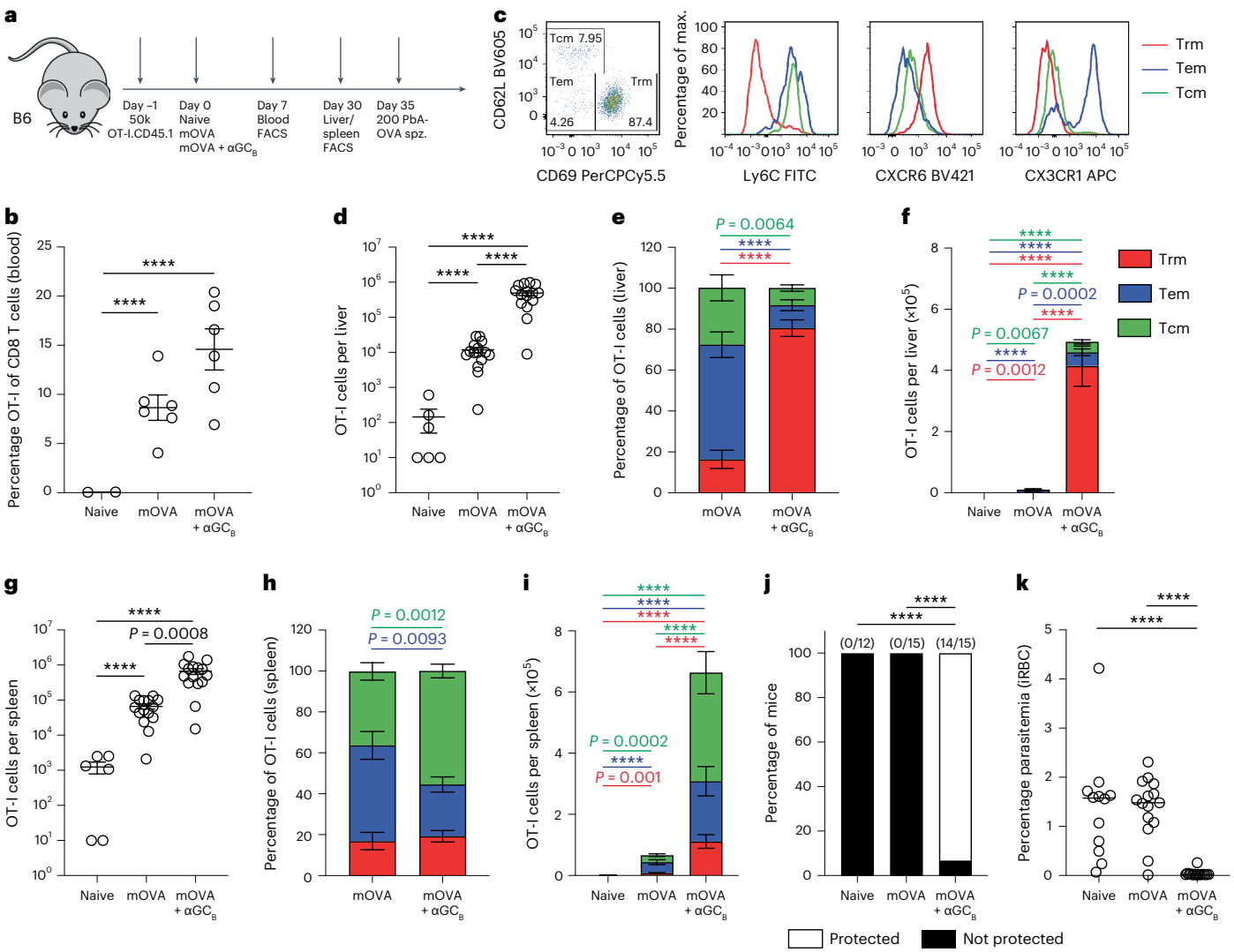

Fig. 1 | Adjuvanted mRNA vaccines can induce liver Trm cells and protect against sporozoite challenge. a, Scheme of experiment. Female B6 mice underwent transfer of 50,000 OT-I.CD45.1 cells 1 day before vaccination with a lipoplex vaccine containing 5 µg mRNA encoding mOVA alone or with adjuvant αGC_B. Gating parameters for analysis of OT-I cells are shown in Supplementary Fig. 1. **b**, Percentages of OT-I cells within CD8 T cells of the blood assessed by flow cytometry on day 7 postvaccination. Values for individual mice are shown, with mean ± s.e.m., reflecting combined data from two independent experiments with one naive mouse and three vaccinated mice per group. **c**, Expression of various cell surface markers on OT-I T cells isolated from the livers of mice vaccinated with mOVA + αGC_B on day 30. **d**–**f**, OT-I cells in the liver: total OT-I cells per liver (mean ± s.e.m.) with individual values shown (**d**), percentage of each memory T cell subset (mean ± s.e.m.) (**e**) and cell counts for each subset (mean ± s.e.m.) (**f**). Data are combined from three experiments, each with two naive mice and five vaccinated mice per group. Individual values for **e** and **f** are shown in Supplementary Fig. 2. **g**–**i**, Analysis of OT-I cells in spleen: total OT-I cells (mean ± s.e.m.) with individual values shown (**g**), percentage of each memory T cell subset (mean ± s.e.m.) (**h**), and cell counts for each subset (mean ± s.e.m.) (**i**). Individual values for **h** and **i** are shown in Supplementary Fig. 2. **j**, Percentages of mice protected (white) or not protected (black) against challenge with 200 OVA-expressing PbA sporozoites, as measured by blood parasitemia up to day 12 postchallenge. Numbers above bars indicate numbers protected of total mice challenged, derived from three independent experiments. **k**, Blood parasitemia at day 7 after sporozoite challenge for mice shown in **j**, presented as percentage of infected RBC (iRBC) per mouse; values for individual mice are shown, with mean ± s.e.m. Data shown in **b**, **d**, **f**, **g**, **i** and **k** were log-transformed and compared using one-way analysis of variance (ANOVA) with Tukey's multiple comparison post-test. Subset data in **e** and **h** were compared by two-sided unpaired Student's *t*-tests. Groups in **j** were compared using Fisher's exact test. Individual *P* values for significant differences are shown, colored to correspond to memory T cell subsets where relevant; ****$P < 0.0001$. max., maximum; spz., sporozoites.

(Fig. 2d–g) and spleen (Extended Data Fig. 1), as indicated by enhanced downregulation of their TCR complex (Fig. 2d,e and Extended Data Fig. 1a,c) and upregulation of PD-1 (Fig. 2f,g and Extended Data Fig. 1b,d) at this memory time point, effects that were also seen with αGC_B. To confirm that liver CD8 Trm cell induction by the αGC_B-adjuvanted mRNA vaccine was indeed NKT cell dependent, we compared memory OT-I CD8 T cell responses in the livers of wild-type and *Traj18*$^{-/-}$ B6 mice, the latter lacking type I NKT cells. Only mice containing type I NKT cells were able to generate efficient liver Trm cell responses (Fig. 2h). Examination of the binding interaction between the TCR of a murine type I NKT cell and murine CD1d complexes containing αGC_B showed a K_d of 39.3 ± 13.9 nM (Extended Data Fig. 2), revealing a modestly higher affinity than we previously reported for αGC (K_d = 102 nM)[31], potentially explaining the improved adjuvancy of αGC_B.

Further mechanistic analysis showed that liver OT-I Trm cell responses induced by αGC_B-adjuvanted mRNA vaccination were dependent on CD40 and type 1 conventional dendritic cells (cDC1), as indicated by impaired responses in *Cd40*$^{-/-}$ and *Batf3*$^{-/-}$ mice,

https://doi.org/10.1038/s41590-023-01562-6

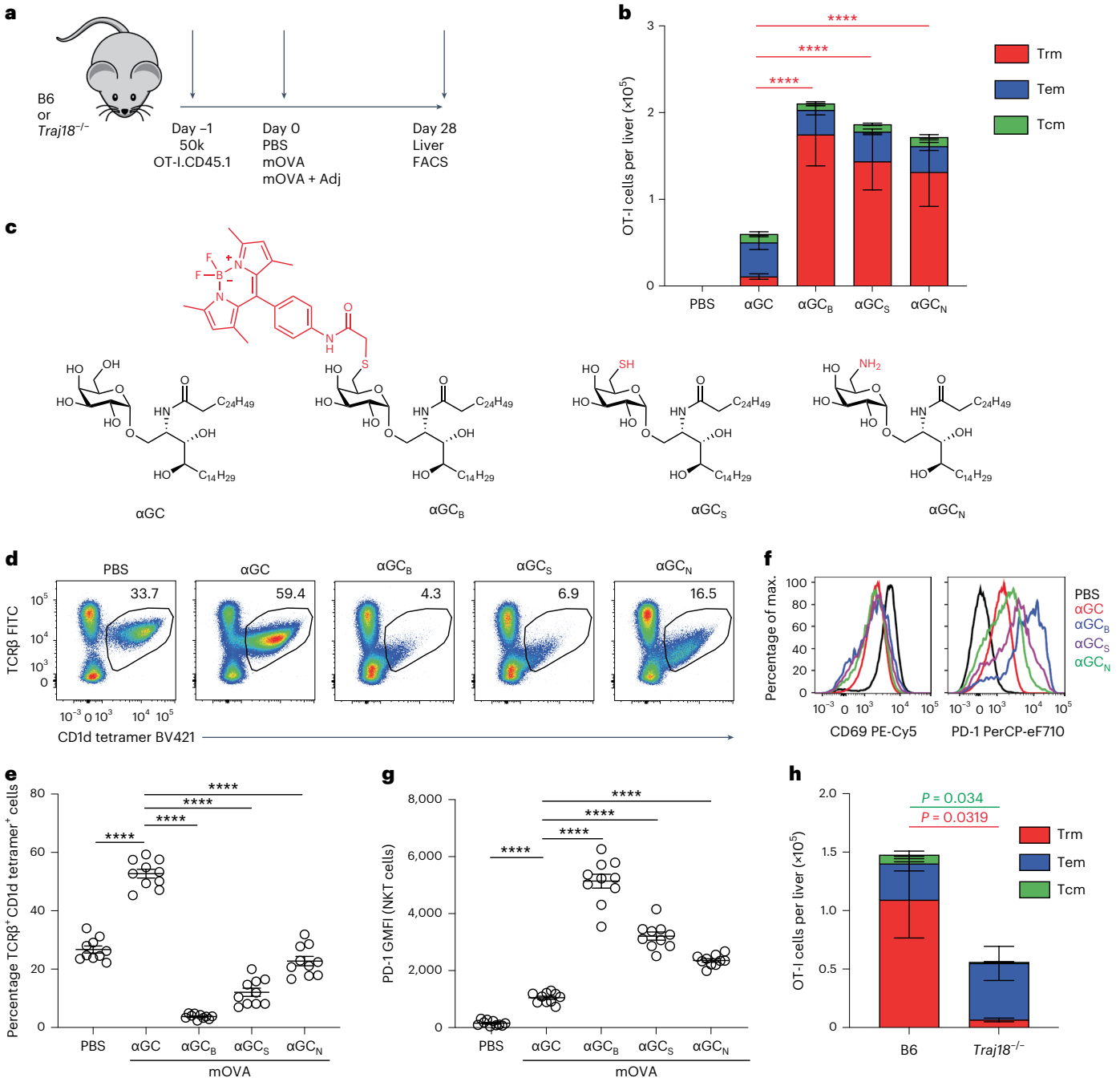

Fig. 2 | Defining the ideal adjuvant for liver Trm cell induction. a, Scheme of experiment. Male B6 mice received transfer of OT-I CD45.1 cells 1 day before vaccination with mOVA vaccine alone or with 80 pmol of the indicated adjuvants. Data in **b**, **e** and **g** are combined from two independent experiments, giving $n = 10$ mice per group. **b**, Cell count (mean ± s.e.m.) for each memory T cell subset in the liver at day 28. Data from vaccinated groups (that is, excluding the PBS group) were log-transformed and then compared by one-way ANOVA with Tukey's multiple comparison post-test; $^{****}P < 0.0001$. Individual counts for each mouse are shown in Supplementary Fig. 3a. **c**, Chemical structures of the adjuvants (created using ChemSketch). **d**, Example flow cytometry plots showing expression of TCR on liver NKT cells at day 28. Gating for NKT cells is shown in Supplementary Fig. 4. **e**, Percentages of liver NKT cells (TCRβ$^+$ CD1d-tetramer$^+$) at day 28, displayed as mean ± s.e.m., with individual values shown. Groups were compared with the αGC group by one-way ANOVA with Dunnett's multiple comparison post-test; $^{****}P < 0.0001$. **f**, Examples of CD69 (left) and PD-1 (right) expression on liver NKT cells. **g**, Geometric mean fluorescence intensity (GMFI) of PD-1 on liver NKT cells. Data are displayed as mean ± s.e.m., and groups were compared with the αGC group by one-way ANOVA with Dunnett's multiple comparison post-test; $^{****}P < 0.0001$. **h**, Analysis of OT-I memory subsets in male B6 ($n = 8$) or *Traj18*$^{-/-}$ mice ($n = 7$) vaccinated with mOVA + αGC$_B$. Cell counts (mean ± s.e.m.) for each memory subset are shown. Data were log-transformed then compared by two-sided unpaired Student's *t*-tests. *P* values are shown for significance tests, colored to correspond to the memory T cell subsets compared. Individual cell counts for each mouse are shown in Supplementary Fig. 3b.

respectively (Fig. 3a,b). Antibody-mediated blocking of CD40L during the priming phase also impaired responses (Fig. 3c, first two bars), although not as efficiently as in *Cd40*$^{-/-}$ mice. MHC II$^{-/-}$ mice (IA$^{-/-}$), which lack CD4 T cells, responded to the adjuvanted vaccine (Fig. 3c, third bar), indicating that CD4 T cells are not essential for this response. However, the response in these animals could be impaired by blocking of CD40L (Fig. 3c, fourth bar), consistent with the CD40L signal originating from NKT cells activated by αGC$_B$. Splenectomy partially

https://doi.org/10.1038/s41590-023-01562-6

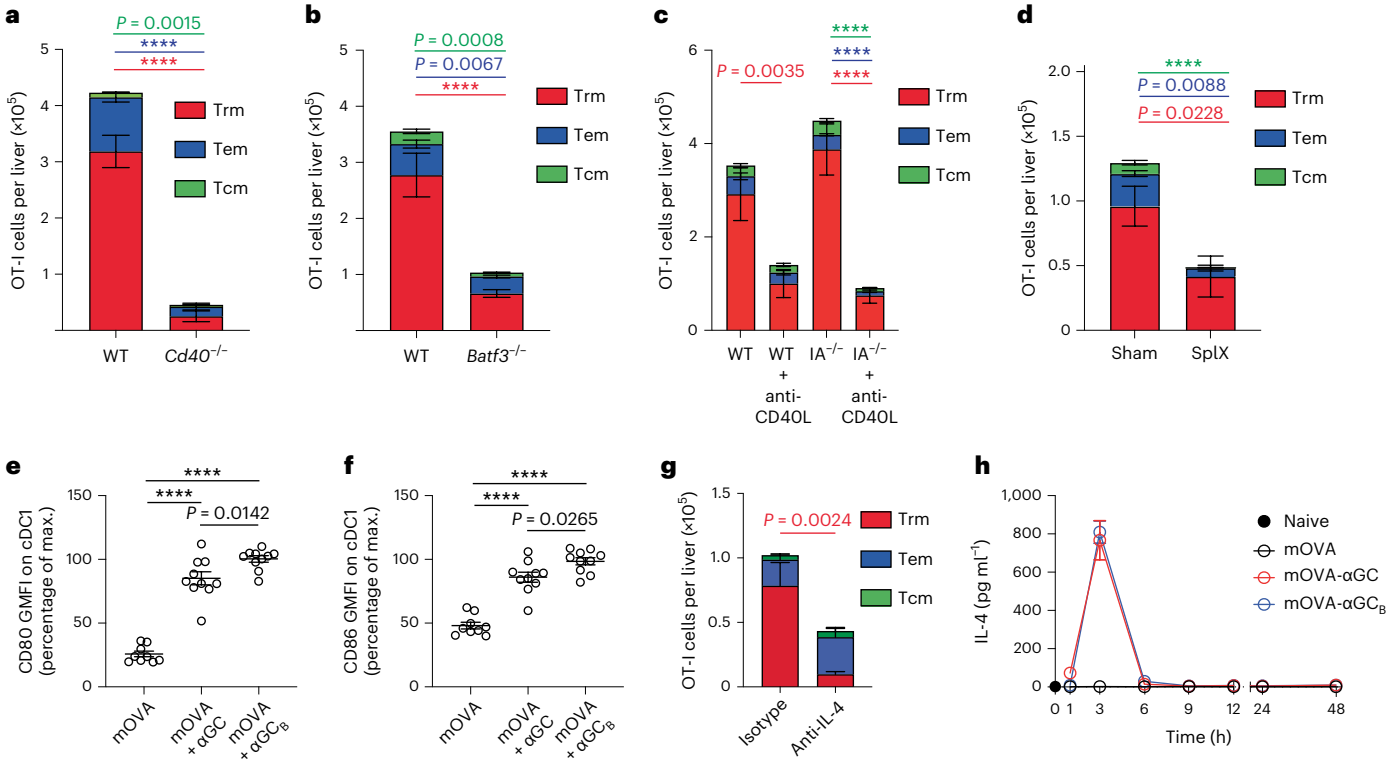

Fig. 3 | Dissection of the mechanistic basis for vaccine activity. a,**b**, Female B6 mice ($n = 10$) and male *Cd40*$^{-/-}$ mice ($n = 7$) (**a**), or female B6 mice ($n = 10$) and female *Batf3*$^{-/-}$ mice ($n = 10$) (**b**), received transfer of 50,000 OT-I.CD45.1 cells 1 day before vaccination with mOVA + αGC_B, and memory OT-I T cell subsets were quantified in liver 28–34 days later. Sample sizes and analyses were generated by combining two independent experiments. Cell counts are shown as mean ± s.e.m. **c**, Analysis of vaccine-induced OT-I memory subsets in female B6 mice versus male and female IA$^{-/-}$ mice with or without treatment with anti-CD40 ligand monoclonal antibody (mAb) or isotype control (wild type (WT) and IA$^{-/-}$ + αCD40L, $n = 10$ per group; WT + αCD40L and IA$^{-/-}$, $n = 9$ per group; derived by combining two experiments). Cell counts are shown as mean ± s.e.m. **d**, Analysis of vaccine-induced OT-I memory subsets in male B6 mice that had been either splenectomized (Splx; $n = 9$) or sham treated ($n = 10$) 7 days before vaccination; data from two combined experiments. Mean ± s.e.m. for cell counts are shown. **e**,**f**, Male B6 mice ($n = 9$ mOVA, $n = 10$ mOVA + αGC/αGC_B per group) were vaccinated with mOVA alone or with adjuvant αGC or αGC_B; 24 h later, splenic cDC1 cells were assessed for expression of CD80 (**e**) and CD86 (**f**). The gating strategy is shown in Supplementary Fig. 5. Data were combined from two experiments and expressed as the percentage of maximum (% of max.), determined by dividing the GMFI of each sample by the maximum mean GMFI of the highest mean of all groups from each experiment. The mean ± s.e.m. is shown. **g**, Analysis of vaccine-induced OT-I memory subsets in male B6 mice treated with IL-4-blocking mAb ($n = 10$) or an isotype control ($n = 9$); data from two combined experiments. Mean ± s.e.m. of cell count is shown. **h**, Serum IL-4 levels (mean ± s.e.m.) in male B6 mice at the indicated times after vaccination with mOVA alone or with adjuvant αGC or αGC_B. Data from a single experiment ($n = 5$ per group) representative of two are shown. Data were log-transformed and compared by two-sided unpaired Student's *t*-tests (**a**, **b**, **d** and **g**) or one-way ANOVA with Tukey's multiple comparison post-test (**c**). Data in **e** and **f** were compared by one-way ANOVA with Tukey's multiple comparison post-test. *P* values are shown; ****$P < 0.0001$. Individual values for data in bar graphs are shown in Supplementary Fig. 6.

impaired the liver CD8 T cell response (Fig. 3d), suggesting that this organ is the major site for priming. Assessment of costimulatory molecule expression by splenic cDC1 (Fig. 3e,f) and liver cDC (Extended Data Fig. 3) 24 h after vaccination showed that both αGC_B and αGC increased CD80 and CD86 expression; αGC_B induced the greatest increase, consistent with its improved capacity to activate NKT cells. Finally, assessment of cytokine dependence during the priming phase using blocking antibodies revealed a significant role for IL-4 (Fig. 3g), a cytokine induced by both αGC and αGC_B very early after immunization (Fig. 3h). No significant role for IL-15, IL-12, IFN-γ or GM-CSF was apparent during priming (Extended Data Fig. 4a); however, as expected, *Il15*$^{-/-}$ mice did not maintain a liver memory T cell response (Extended Data Fig. 4b), as this cytokine is essential for memory T cell survival[32]. Inhibition of type I IFN signaling appeared to moderately enhance responses (Extended Data Fig. 4c). Taken together, these data suggest that addition of αGC_B to the mRNA vaccine leads to induction of an NKT cell-dependent response that signals CD40 on cDC1 to increase costimulation for CD8 T cells. It also induces NKT cell-derived cytokines, particularly IL-4, that help generate a liver CD8 T cell response. Notably, IL-4 dependence of the CD8 T cell response to malaria sporozoites has been reported[33].

Endogenous liver Trm induction

All work described up to this point was conducted in mice with adoptive transfer of OT-I cells for ease of cell tracking. To assess whether endogenous T cells were also able to generate liver Trm cells in response to adjuvanted mRNA vaccines, B6 mice were vaccinated with mOVA vaccines alone or incorporating αGC or αGC_B and then examined for antigen-specific effector and memory CD8 T cell responses by staining with MHC–peptide pentamers (Fig. 4a). On day 7, the blood from each group contained a high proportion of OVA-specific CD8 T cells (Fig. 4b). After 30 days, however, significantly more OVA-specific liver Trm cells were evident in mice that had received the αGC_B-adjuvanted mRNA vaccine, although those receiving αGC also showed moderate induction (Fig. 4c). The spleens and lungs of mice receiving adjuvanted vaccines also showed increased memory T cell numbers, although these were largely Tem cells, with few Trm cells found in either tissue (Fig. 4d,e).

To explore whether the difference between αGC_B and αGC in terms of their capacity to induce liver Trm cells was a consequence of the available dose of the NKT cell adjuvant, we examined the endogenous response to OVA using a range of doses of each adjuvant incorporated into our vaccines (Fig. 4f). Although responses to both adjuvants

https://doi.org/10.1038/s41590-023-01562-6

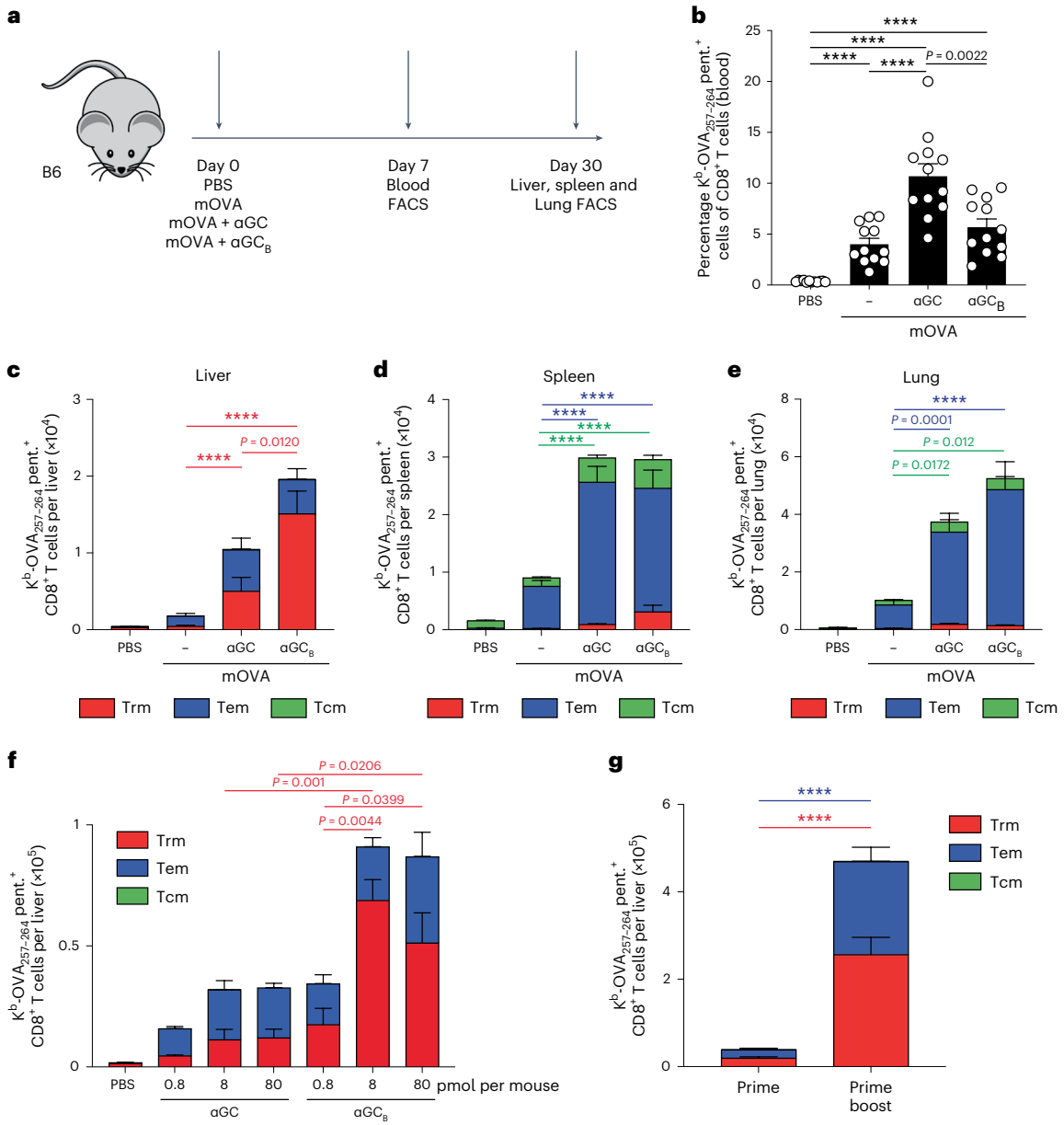

Fig. 4 | Endogenous T cell response to adjuvanted mRNA vaccination. **a**, Scheme of experiments in **b**–**f**. Male B6 mice were vaccinated i.v. with mOVA alone or with adjuvants αGC or αGC$_B$. **b**, Percentages of CD8 T cells that were OVA$_{257-264}$ specific in blood on day 7 postvaccination, with mean ± s.e.m. Gating parameters are described in Supplementary Fig. 9. Data were log-transformed and compared by one-way ANOVA with Tukey's multiple comparison post-test. **c**–**e**, Assessment of total number of each memory T cell subset of OVA$_{257-264}$-specific T cells on day 30 in the liver (**c**), spleen (**d**) and lung (**e**). Data were combined from two independent experiments, giving $n = 12$ mice per group, displayed as mean cell count ± s.e.m. Data from vaccinated groups (that is, excluding the PBS group) for Trm cell numbers in **c** and for Tem or Tcm cell numbers in **d** and **e** were log-transformed then compared by one-way ANOVA with Tukey's multiple comparison post-test. Individual values for each mouse in **c**–**e** are shown in Supplementary Fig. 10a–c. **f**, Total number of each memory T cell subset of OVA$_{257-264}$-specific T cells in the liver 30 days after vaccination with mOVA together with titrated dose of αGC or αGC$_B$ (0.8–80 pmol). Data are presented as mean ± s.e.m. from one experiment ($n = 5$ per group). Data were log-transformed, and Trm counts from the αGC and αGC$_B$ groups were compared by one-way ANOVA with Tukey's multiple comparison post-test. For simplicity, statistical differences between the two adjuvants at different doses are not shown. Individual values for each mouse in **f** are shown in Supplementary Fig. 10d. **g**, Total number of each subset of OVA$_{257-264}$-specific T cells in the liver on day 60 after initial priming with mOVA + αGC$_B$ ($n = 15$ prime, $n = 13$ prime–boost), with or without homologous boosting at day 30. Sample size and analysis generated from combining two independent experiments. Cell count is shown as mean ± s.e.m. Data were log-transformed then compared using two-sided unpaired Student's *t*-tests. Individual values for each mouse are shown in Supplementary Fig. 10e. pent., pentamer.

plateaued at about 8 pmol per mouse, αGC$_B$ induced more liver Trm cells than αGC, suggesting that this modification was more efficacious.

Finally, to assess whether endogenous T cell responses to αGC$_B$-adjuvanted mRNA could be boosted, B6 mice were primed and then boosted on day 30 and examined for liver CD8 Trm cell responses on day 60 (Fig. 4g). This revealed a significant increase in OVA-specific liver Trm cells following boosting, together with an increase in circulating Tem cells in the liver. Although our primary goal was to assess induction of liver Trm cells, antibody responses can impair liver-stage infection when target antigens are expressed on the sporozoite surface[11]. It was therefore noteworthy that serum OVA-specific antibody responses were induced in a prime–boost

https://doi.org/10.1038/s41590-023-01562-6

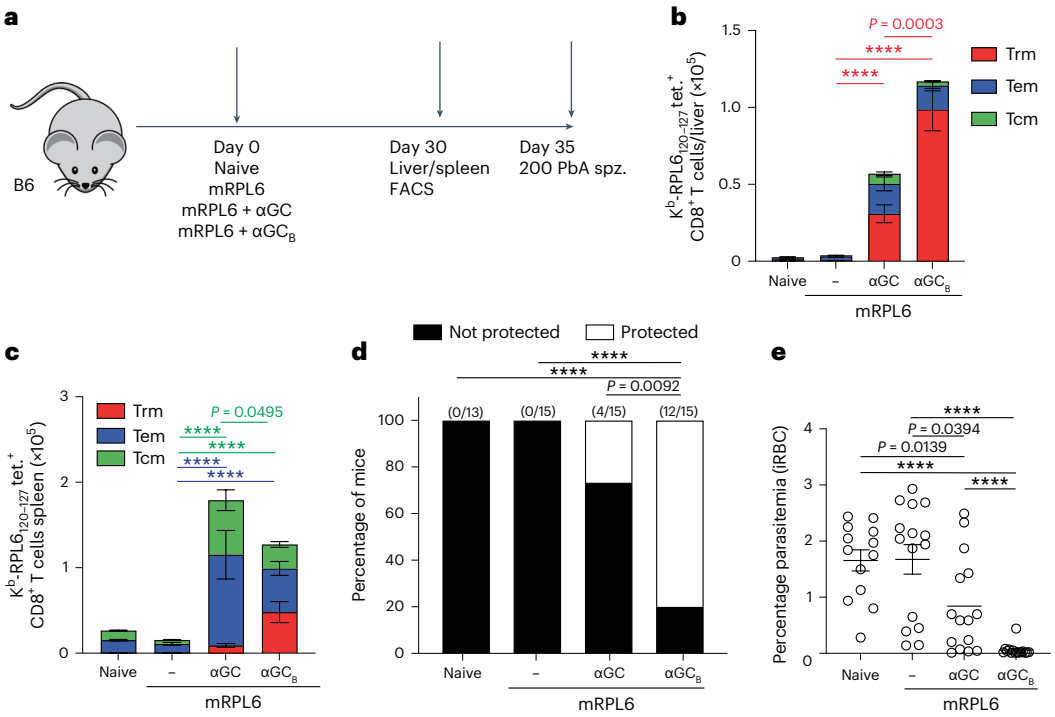

Fig. 5 | Vaccination with adjuvanted mRNA can induce protection against an authentic parasite antigen. a, Scheme of experiment. Female B6 mice were vaccinated i.v. with 5 µg of mRPL6 alone or with αGC or αGC$_B$. Memory T cell responses were measured 30 days later, with the gating parameters described in Supplementary Fig. 11. **b**,**c**, K^b-RPL6$_{120–127}$ memory CD8 T cell subsets in the liver (**b**) and spleen (**c**). Data are presented as mean ± s.e.m. cell count per subset from four independent experiments ($n = 3$ total for naive group; $n = 18$, mRPL6 alone; $n = 19$, mRPL6 + αGC; $n = 19$, mRPL6 + αGC$_B$). Trm cell data (**b**) and Tem and Tcm cell data (**c**) from vaccinated groups were log-transformed and compared by one-way ANOVA with Tukey's multiple comparison post-test. Individual values for each mouse in **b** and **c** are shown in Supplementary Fig. 12. **d**, Percentages of mice protected (white) and not protected (black) against a challenge with 200 PbA sporozoites on day 35, as measured by blood parasitemia up to day 12. Numbers above bars indicate the proportions of protected mice to total mice, accumulated from three independent experiments. Data were analyzed using Fisher's exact test. **e**, Blood parasitemia at day 7 after sporozoite challenge in mice from **d**. Percentages of iRBC for individual mice are shown, with mean ± s.e.m. per group. Data were log-transformed and compared by one-way ANOVA with Tukey's multiple comparison post-test. ****$P < 0.0001$.

setting, although addition of either NKT cell agonist appeared to reduce potency (Extended Data Fig. 5).

Induction of Trm cells to PbA antigens

To assess the capacity of αGC$_B$-adjuvanted vaccines to protect against malaria challenge under conditions where an authentic malaria antigen was used, we generated an mRNA lipoplex vaccine encoding the large ribosomal subunit protein L6 (RPL6) of *P. berghei*. The gene for RPL6 is highly conserved, showing almost no strain polymorphism in the human pathogen *P. falciparum*[34], making it ideal for vaccine development. Mice were vaccinated with the RPL6–mRNA vaccine (mRPL6) alone or adjuvanted with either αGC or αGC$_B$ and then examined for memory T cell responses in the spleen and liver (Fig. 5a–c). This revealed superior induction of RPL6$_{120–127}$-specific liver Trm cells by the αGC$_B$-adjuvanted vaccine (Fig. 5b), with αGC also inducing some liver Trm cells, and both adjuvants increasing circulating T cell responses in the spleen (Fig. 5c). To assess whether these vaccines protected against sporozoite challenge, mice were infected with 200 PbA sporozoites and assessed for onset of blood-stage infection (Fig. 5d,e). Eighty per cent of mice given the αGC$_B$-adjuvanted vaccine showed no parasitemia and were thus sterilely protected. By contrast, neither the αGC-adjuvanted vaccine nor the vaccine lacking the NKT cell agonist was highly protective. The αGC-adjuvanted vaccine did, however, prevent infection in 26% of mice, with most mice showing a reduction in blood-stage parasitemia on day 7 (Fig. 5e), indicative of a partially protective response in the liver. Overall, these data show that the αGC$_B$-adjuvanted mRNA vaccine encoding RPL6 is highly protective.

Protection depends on liver Trm cells

Next, we showed that RPL6-specific liver Trm cell numbers could be further increased by antigen-specific boosting after 30 days (Fig. 6a). Boosting also increased the number of circulating memory T cells in the spleen (Fig. 6b) and protected a high proportion of mice from challenge with 200 PbA sporozoites (Fig. 6c). To explore whether protection was mediated by liver Trm cells and/or circulating memory T cells, we first confirmed that it was mediated by CD8 T cells. B6 mice were primed with an αGC$_B$-adjuvanted mRPL6 vaccine and treated ~30 days later with depleting monoclonal antibodies specific for either CD8 or a combination of CD4 and NK1.1, to deplete either CD8 T cells alone or the group of CD4 T cells, NKT cells and NK cells (Fig. 6d). Upon challenge with 200 PbA sporozoites, protection was ablated in the CD8 T cell-depleted group only (Fig. 6e), indicating that CD8 T cells but not CD4 T cells, NKT cells or NK cells are essential effectors of protection.

To determine the subset(s) of CD8 T cells responsible for protection, vaccinated mice were depleted of Trm cells by injection of a monoclonal antibody against the surface marker CXCR3, as previously described[8], or were depleted of circulating T cells by injection of an anti-Gr-1 monoclonal antibody, as previously described[35] (Fig. 7a–c). When these mice were challenged with 200 PbA sporozoites, they all maintained effective protection except those depleted of liver Trm cells (Fig. 7d,e), indicating a major role for liver CD8 Trm cells in this protection.

No impairment by previous parasitemia

Previous studies have shown that exposure to the blood stage of malaria can have detrimental effects on the ability to generate

https://doi.org/10.1038/s41590-023-01562-6

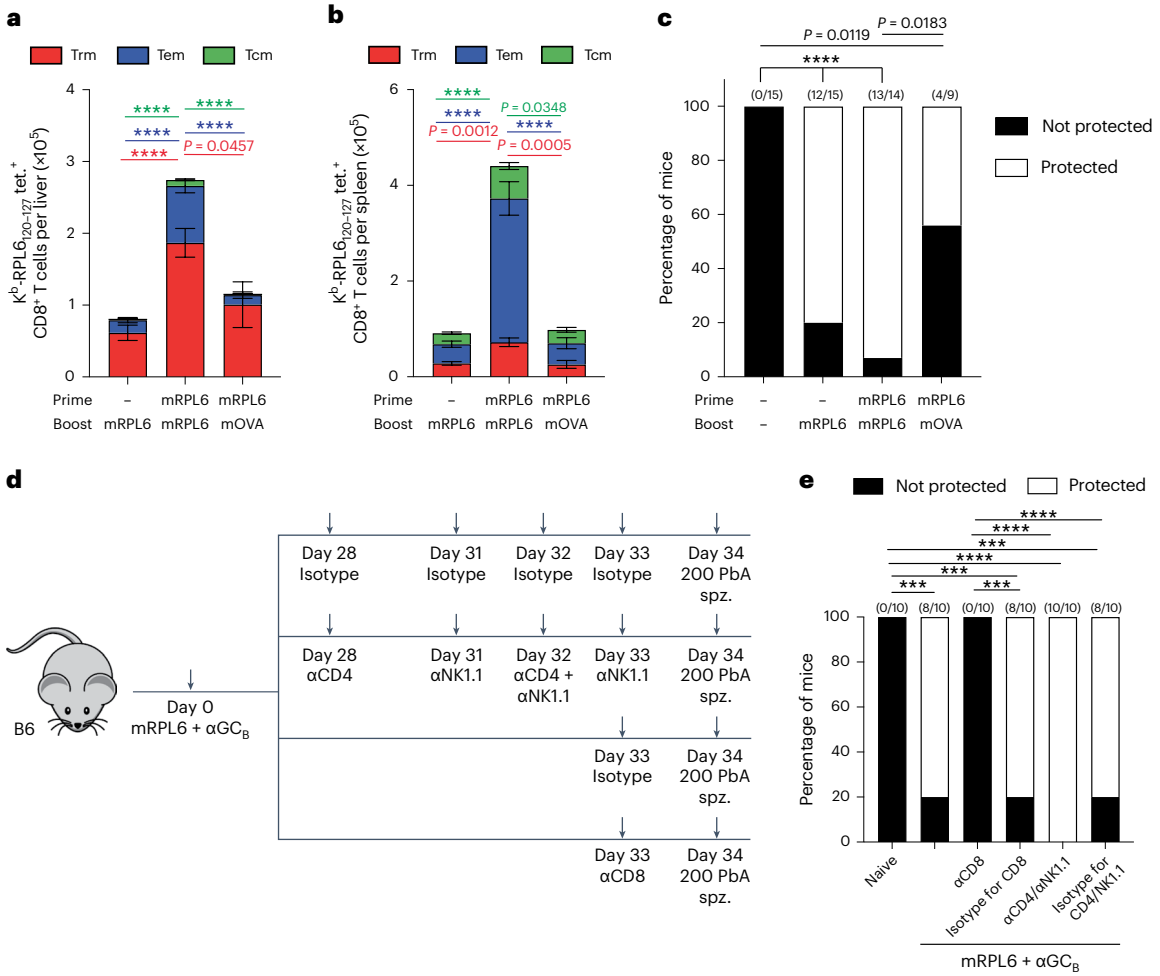

Fig. 6 | Protective responses can be boosted and require CD8 cells. a,**b**, Female B6 mice were vaccinated with mRPL6 + αGC_B vaccine and boosted 30–60 days later with either mRPL6 + αGC_B (homologous prime–boost) or mOVA + αGC_B (heterologous), or primed for the first time with mRPL6 + αGC_B. Memory T cell responses were measured in a subset of mice 30 days after boosting ($n = 24$ mice for the homologous vaccine group; $n = 9$ for the heterologous group; $n = 23$ for the prime-only group; derived by combining 2–4 independent experiments). The remaining mice were challenged with 200 PbA sporozoites to assess vaccine efficacy. K^b-$RPL6_{120–127}$ memory CD8 T cell responses were assessed in the liver (**a**) and spleen (**b**). Data are presented as mean ± s.e.m. of cell count. **c**, Proportions of mice protected (white) and not protected (black) against challenge with 200 PbA sporozoites as measured by blood parasitemia up to day 12. Numbers above bars indicate the numbers of protected mice from 2–3 independent experiments. Data in **a** and **b** were log-transformed and compared by one-way ANOVA with Tukey's multiple comparisons post-test. Groups in **c** were compared using Fisher's exact test. In one challenge experiment ($n = 5$), no mice including those in naive control groups became infected; data from this experiment were not included, but mice were rechallenged with viable sporozoites on day 69, and these data were included in the pooled data; $^{****}P < 0.0001$. Individual values for each mouse in **a** and **b** are shown in Supplementary Fig. 13a,b. **d**, Scheme of experiment shown in **e**. Groups of B6 mice ($n = 10$) were primed with mRPL6 + αGC_B vaccine and then either depleted of CD8 T cells using anti-CD8 antibodies or depleted of CD4, NK and NKT cells using anti-CD4 and anti-NK1.1 antibodies, with control groups of mice treated with the relevant isotype control antibodies. Thirty-four days after priming, mice were challenged with 200 PbA sporozoites. **e**, Percentages of mice protected (white) and not protected (black) against sporozoite challenge as measured by blood parasitemia up to day 12. Numbers above bars indicate the proportions of protected mice to total mice from two independent experiments. Groups were compared using Fisher's exact test; $^{****}P < 0.0001$.

liver-stage-specific immunity[20]. We confirmed this here by examining the response of OT-I cells to radiation-attenuated sporozoites (RAS) expressing OVA (Fig. 8a,b). Mice were either left untreated or were first exposed to blood-stage *Plasmodium chabaudi* infection for 1 month before clearing of parasites by treatment with chloroquine. Infection with *P. chabaudi* was used instead of PbA as, unlike PbA, it does not cause acute lethal infection. Nine days after treatment to cure *P. chabaudi* blood-stage infection, mice underwent adoptive transfer of naive OT-I cells and were then vaccinated with OVA-expressing RAS to examine induction of memory OT-I populations in the liver. A dramatic reduction in T cell responses was observed in *P. chabaudi* blood-stage-exposed mice (Fig. 8b), consistent with published findings[20]. This type of impaired immunity is potentially highly deleterious to the vaccination of humans in malaria-endemic regions and may explain the disappointing efficacy of attenuated sporozoite vaccines in the field compared with the success seen in controlled trials in naive humans[17–19]. To determine whether liver Trm cell responses induced by an αGC_B-adjuvanted mRNA vaccine were also affected by previous blood-stage exposure, mice pretreated as above were vaccinated with an αGC_B-adjuvanted mOVA vaccine, and liver memory T cell responses were examined (Fig. 8a,c). Similar induction of liver Trm cell populations was seen in the two groups of mice. To ensure that responses induced after blood-stage infection were functional, mRNA-vaccinated mice were challenged with 200 OVA-expressing PbA sporozoites, revealing effective protection despite preexposure to blood-stage malaria (Fig. 8d,e). Together, these results indicate that the suppressive effects of blood-stage preexposure seen for attenuated sporozoite vaccines do not extend to immunization by adjuvanted

https://doi.org/10.1038/s41590-023-01562-6

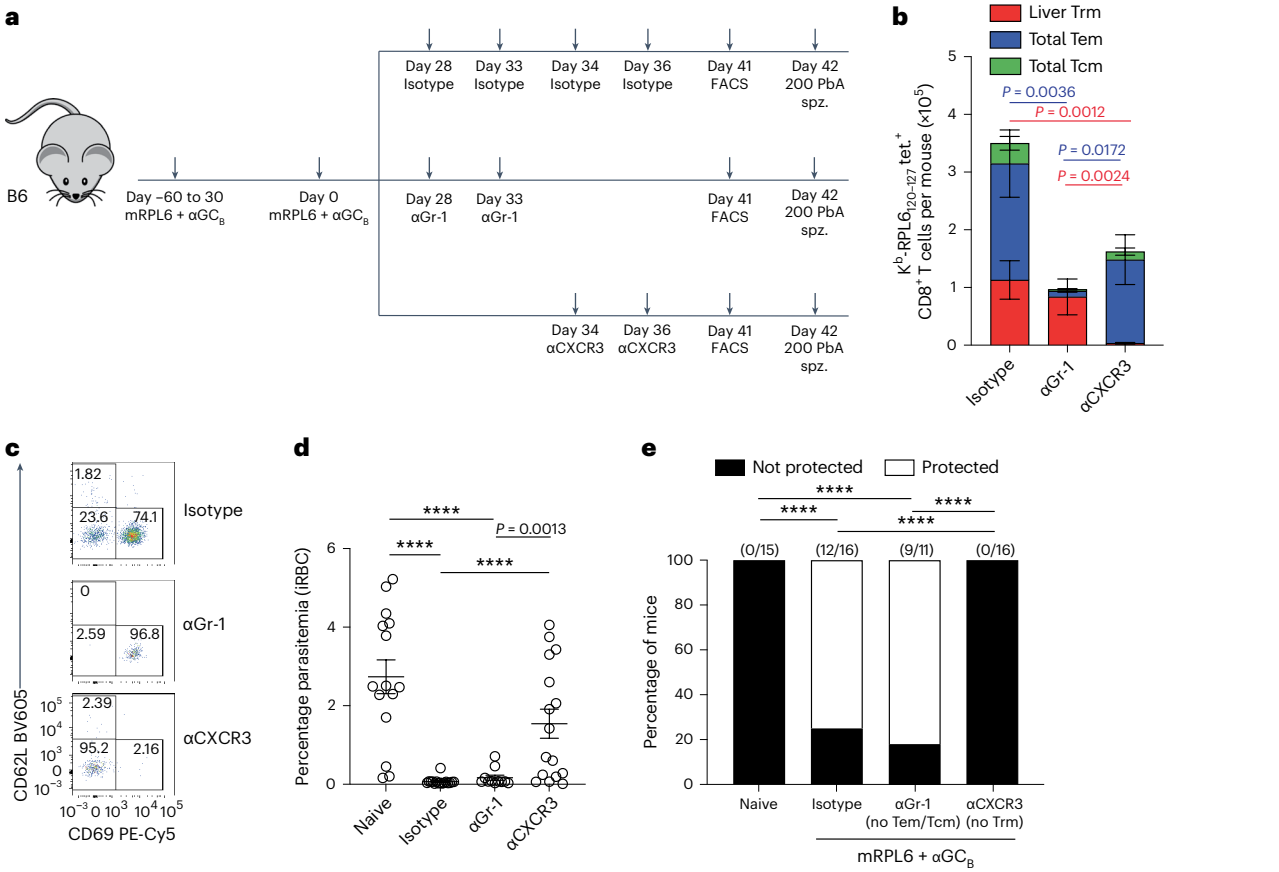

Fig. 7 | Protection is largely dependent on liver Trm cells. a, Scheme of experiment shown in **a**–**e**. Female B6 mice were primed and boosted with mRPL6 + αGC_B vaccine, with a 30–60 day interval. Boosted mice were depleted of either Tem and Tcm cells using anti-Gr-1 or Trm cells using anti-CXCR3 antibodies, and control mice were treated with isotype antibodies. Memory T cell responses were measured in the spleen and liver in a subset of mice 41 days after boosting, and the remaining mice were challenged with 200 PbA sporozoites. **b**, K^b-$RPL6_{120–127}$ memory CD8 T cell numbers for liver Trm cells and combined liver + spleen (total) Tem and Tcm cells ($n = 6$ mice for isotype group; $n = 4$, anti-Gr-1; $n = 7$, anti-CXCR3; derived from 2–3 independent experiments). Data are displayed as mean ± s.e.m. and were log-transformed and compared by one-way ANOVA with Tukey's multiple comparison post-test. Individual values for each mouse in **b** are shown in Supplementary Fig. 13c. **c**, Phenotype of K^b-$RPL6_{120–127}$ memory CD8 T cells in the liver. **d**, Blood parasitemia at day 7 after 200 PbA sporozoite challenge ($n = 15$ naive mice; $n = 16$, isotype; $n = 11$, anti-Gr-1; $n = 16$, anti-CXCR3; derived from three combined experiments). Data are displayed as mean ± s.e.m. with points for individual mice shown. Data were log-transformed and compared by one-way ANOVA with Tukey's multiple comparison post-test; $^{****}P < 0.0001$. **e**, Percentages of mice protected (white) and not protected (black) against sporozoite challenge as measured by blood parasitemia up to day 12. Numbers above bars indicate proportions of protected to total mice. Fisher's exact test; $^{****}P < 0.0001$.

mRNA vaccines, potentially a major advantage for translation into the field.

Discussion

The lipoplex mRNA vaccine format used here has previously been shown to prime T cell responses in preclinical models of cancer[36–38] and has been successfully used to induce T cell responses in cancer patients[39]. Those vaccines were administered i.v. to allow mRNA access to antigen-presenting cells within the lymphoid compartment, notably the spleen[40], with multiple doses of vaccine administered over short intervals. In mice, this regimen was typically a minimum of three doses 3–5 days apart; in humans, a minimum of five doses 1 week apart were administered, with the interval then increasing to a monthly booster schedule that—in some cases—reached a full year of treatment. In our study, we also used an i.v. route of administration, which had the added advantage of facilitating access of the vaccines to the NKT cell-rich regions of the spleen and liver. However, in a prophylactic setting, multiple doses over a short interval would be impractical, so we initially evaluated one dose. This regimen was sufficient to induce measurable CD8 T cell responses, irrespective of inclusion of an NKT cell agonist, achieving levels in the blood at day 7 that were in keeping with those reported in a study of a similar OVA-encoding vaccine that used a short-interval two-dose schedule[40]. However, inclusion of 6-modified αGC-based agonists such as αGC_B in the vaccine altered memory formation, resulting in significantly enhanced accumulation of liver Trm cells by day 30. Furthermore, a homologous prime and boost, using a more practical extended interval of at least a month, was able to substantially increase T cell responses while retaining a strong propensity for liver Trm induction. Using our adjuvanted vaccine, we were able to tailor immunity toward liver Trm cell generation and achieve substantial sterile protection against sporozoite challenge with a single immunization, but protection was improved by boosting.

Although modest protection against sporozoite challenge has been reported for a lipid-nanoparticle-based mRNA vaccine encoding *P. falciparum* circumsporozoite protein, this approach required multiple vaccinations for efficacy and was designed with antibody generation as its primary effector mechanism[41]. No assessment of liver Trm cells was undertaken; however, given our results with unadjuvanted vaccine here, induction of this T cell subset was likely to have been poor. By contrast, adjuvanting an mRNA vaccine with an NKT cell agonist to favor liver Trm cell generation allowed us to achieve high levels of sterile protection with a single dose of vaccine and even greater protection

https://doi.org/10.1038/s41590-023-01562-6

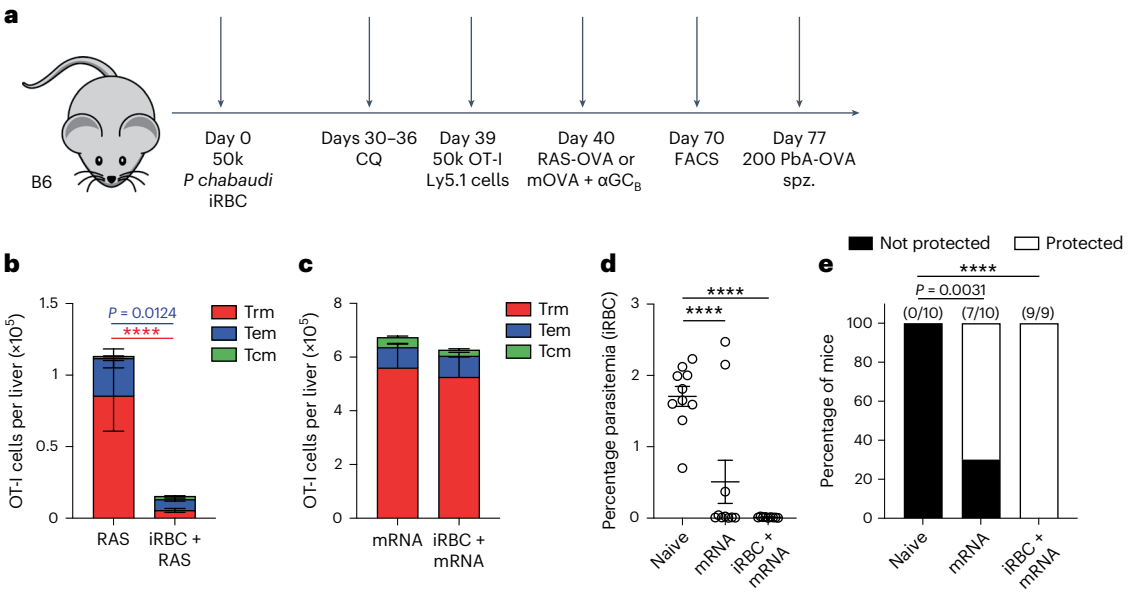

Fig. 8 | Vaccination with adjuvanted mRNA is not impaired by preexposure to blood-stage malaria. a, Scheme of experiment. Female B6 mice were left untreated or infected i.p. with 50,000 *P. chabaudi* parasitized RBC (iRBC) then treated with chloroquine (CQ) from days 30–36 to remove residual parasites. On day 39, pretreated and naive mice received adoptive transfer of 50,000 purified OT-I.CD45.1 cells; the mice were vaccinated the following day with either 50,000 irradiated OVA-expressing sporozoites (RAS) or mOVA + αGC$_B$ vaccine. Memory T cell responses were measured in a subset of mice 30 days after priming, and the remaining mice were challenged with 200 PbA sporozoites to assess vaccine efficacy. **b**, Total numbers of OT-I cells in the livers of RAS-vaccinated mice ($n = 15$ mice for RAS-only group, $n = 13$ for iRBC + RAS; derived by combining three independent experiments). Data are displayed as mean ± s.e.m. **c**, Total numbers of OT-I cells in the livers of lipoplex mRNA-vaccinated mice ($n = 15$ mice for mRNA vaccine alone, $n = 14$ for iRBC + mRNA vaccine; derived by combining three independent experiments). Data are displayed as mean ± s.e.m. Data in **b** and **c** were log-transformed and compared using two-sided unpaired Student's *t*-tests. Individual values for each mouse in **b** and **c** are shown in Supplementary Fig. 14. **d**, Blood parasitemia at day 7 after challenge with 200 PbA sporozoites ($n = 10$ mice for naive group, $n = 10$ for mRNA vaccine alone, $n = 9$ for iRBC + mRNA vaccine; derived by combining two independent experiments). Data are displayed as mean ± s.e.m., with points for individual mice shown. Data were log-transformed and compared by one-way ANOVA with Tukey's multiple comparison post-test. *P* values are shown; ****$P < 0.0001$. **e**, Percentages of mice protected (white) and not protected (black) against sporozoite challenge in **d** as measured by blood parasitemia up to day 12. Numbers above bars indicate proportions of protected to total mice. Groups were compared using Fisher's exact test. *P* values are shown; ****$P < 0.0001$.

with subsequent boosting. Although our approach is highly efficacious, it adds a level of complexity for translation, with aspects such as safety and efficacy still to be explored in detail. NKT cell agonists have, however, been used to activate NKT cells in humans[42,43], with evidence of adjuvant activity[44], supporting their translation potential.

The inclusion of unmodified αGC in the vaccine was sufficient to induce enhanced circulating T cell responses (mainly Tem cells) in the blood, spleen, lung and liver. An enhancing effect of including αGC in i.v. administered mRNA vaccines has also been reported in mice[45,46], resulting in improved antitumour activity. However, here we found that unmodified αGC was associated with only a small to modest increase in liver Trm cells, which was generally insufficient to provide overt protection from sporozoite challenge. The use of 6-modified αGC agonists similarly enhanced circulating T cell responses, but the memory responses in liver were markedly different, with proportionally more Trm cells. The modified agonists also induced a qualitatively different NKT cell response to αGC, with sustained downregulation of the TCR–CD3 complex and upregulation of activation markers. As glycolipid agonists accounted for only a minor proportion of the injected lipoplexes (~0.06% mol/mol of lipids), it is unlikely that the modifications caused immediate changes in biodistribution of the injected material that would explain this altered NKT cell activity. We have some evidence for a modest increase in avidity for NKT TCR interactions with αGC$_B$ bound to CD1d, compared with the equivalent for αGC, which may account for the improved adjuvant activity. CD40 signaling, most likely in cDC1, was crucial for induction of liver CD8 T cell responses, with upregulation of CD80 and CD86 on cDC1 cells being probable downstream effects of the CD40 signal. The significant increase in expression of these costimulatory molecules induced by αGC$_B$ relative to αGC may contribute to improved responses. IL-4 also played an important part, though no differences were observed in IL-4 expression or kinetics between agonists. Thus, whereas the enhanced adjuvancy of αGC$_B$ over αGC is reflected in increased NKT cell activation, and increased levels of cDC1 costimulatory molecule expression, improved Trm formation may involve additional and perhaps subtle properties. These could include: cytokine bias[47]; differential release from lipoplexes; differences in processing for loading onto CD1d; or even different clearance rates, where enzymes involved in degradation of αGC may be affected by 6-modifications[48]. Increased stability could lead to more sustained NKT cell responses, with those in the liver then promoting appropriate signals to facilitate local Trm cell formation.

One interesting aspect to come from the assessment of protective effector mechanisms for this vaccine was that despite the relatively large pool of Tem cells generated, protection was largely mediated by Trm cells. Depletion of Trm cells led to a complete loss of sterile immunity, which was unaffected by depletion of Tem cells. Notably, however, the level of parasitemia on day 7 trended lower in the Trm-depleted group compared with the naive controls (although not significantly), potentially suggesting a partial contribution by Tem cells[12] and reiterating the need for generation of large numbers of these cells to achieve substantial protection[49]. Our findings highlight the importance of designing vaccines that favor liver Trm cell induction in the challenge to develop an effective malaria vaccine.

mRNA vaccines are being rapidly implemented and accepted worldwide, facilitating translation of this developing technology. One major advantage of these vaccines is that they provide the opportunity

to include whole parasite genes or even multiple genes, enabling supply of a diverse array of potential immunogenic epitopes to cover the broad spectrum of human HLA. Use of whole genes in mRNA vaccines also enables immunity to be directed to the best antigenic targets, particularly antigens such as RPL6, which shows almost no strain variation[34], avoiding the problems with other more polymorphic antigens, such as thrombospondin-related adhesion protein. It also avoids the complication seen with the use of attenuated sporozoite vaccines, where repeated doses bias immunity to sporozoite-expressed antigens over those expressed in the liver[50]. Finally, as clearly demonstrated here, vaccination with adjuvanted mRNA is not adversely affected by preexposure to blood-stage infection, a major issue with the use of attenuated sporozoite vaccines[20]. It is not clear why preexposure to blood-stage parasites affects immunity generated by irradiated sporozoites, but alteration in dendritic cell function has been proposed[20]. Our own studies have suggested that phagocytosis may be impaired by exposure to blood-stage infection[51], which may not be a critical factor in mRNA vaccination if vaccines simply fuse with presenting cells to introduce mRNA into the cytosol. Whatever the reason, this approach offers hope that some of the factors that make immunization difficult in malaria-endemic regions may be overcome by advances in mRNA vaccination.

Online content

Any methods, additional references, Nature Portfolio reporting summaries, source data, extended data, supplementary information, acknowledgements, peer review information; details of author contributions and competing interests; and statements of data and code availability are available at https://doi.org/10.1038/s41590-023-01562-6.

References

1. World Health Organization. *World Malaria Report 2021*. WHO, 2021.
2. Cowman, A. F., Healer, J., Marapana, D. & Marsh, K. Malaria: biology and disease. *Cell* **167**, 610–624 (2016).
3. Crompton, P. D. et al. Malaria immunity in man and mosquito: insights into unsolved mysteries of a deadly infectious disease. *Annu Rev. Immunol.* **32**, 157–187 (2014).
4. Laurens, M. B. RTS,S/AS01 vaccine (Mosquirix): an overview. *Hum. Vaccin Immunother.* **16**, 480–489 (2020).
5. Duffy, P. E. & Patrick Gorres, J. Malaria vaccines since 2000: progress, priorities, products. *NPJ Vaccines* **5**, 48 (2020).
6. Datoo, M. S. et al. Efficacy and immunogenicity of R21/Matrix-M vaccine against clinical malaria after 2 years' follow-up in children in Burkina Faso: a phase 1/2b randomised controlled trial. *Lancet Infect. Dis.* **22**, 1728–1736 (2022).
7. Datoo, M. S. et al. Efficacy of a low-dose candidate malaria vaccine, R21 in adjuvant Matrix-M, with seasonal administration to children in Burkina Faso: a randomised controlled trial. *Lancet* **397**, 1809–1818 (2021).
8. Fernandez-Ruiz, D. et al. Liver-resident memory CD8$^+$ T cells form a front-line defense against malaria liver-stage infection. *Immunity* **45**, 889–902 (2016).
9. Seder, R. A. et al. Protection against malaria by intravenous immunization with a nonreplicating sporozoite vaccine. *Science* **341**, 1359–1365 (2013).
10. Epstein, J. E. et al. Live attenuated malaria vaccine designed to protect through hepatic CD8$^+$ T cell immunity. *Science* **334**, 475–480 (2011).
11. Schofield, L. et al. γ Interferon, CD8$^+$ T cells and antibodies required for immunity to malaria sporozoites. *Nature* **220**, 664–666 (1987).
12. Lefebvre, M. N. et al. Expeditious recruitment of circulating memory CD8 T cells to the liver facilitates control of malaria. *Cell Rep.* **37**, 109956 (2021).
13. Tse, S. W., Radtke, A. J., Espinosa, D. A., Cockburn, I. A. & Zavala, F. The chemokine receptor CXCR6 is required for the maintenance of liver memory CD8$^+$ T cells specific for infectious pathogens. *J. Infect. Dis.* **210**, 1508–1516 (2014).
14. Holz, L. E. et al. CD8$^+$ T cell activation leads to constitutive formation of liver tissue-resident memory T cells that seed a large and flexible niche in the liver. *Cell Rep.* **25**, 68–79 (2018).
15. Nunes-Cabaco, H., Moita, D. & Prudencio, M. Five decades of clinical assessment of whole-sporozoite malaria vaccines. *Front. Immunol.* **13**, 977472 (2022).
16. Ishizuka, A. S. et al. Protection against malaria at 1 year and immune correlates following PfSPZ vaccination. *Nat. Med.* **22**, 614–623 (2016).
17. Jongo, S. A. et al. Immunogenicity and protective efficacy of radiation-attenuated and chemo-attenuated PfSPZ vaccines in Equatoguinean adults. *Am. J. Trop. Med. Hyg.* **104**, 283–293 (2021).
18. Oneko, M. et al. Safety, immunogenicity and efficacy of PfSPZ vaccine against malaria in infants in western Kenya: a double-blind, randomized, placebo-controlled phase 2 trial. *Nat. Med.* **27**, 1636–1645 (2021).
19. Sissoko, M. S. et al. Safety and efficacy of a three-dose regimen of *Plasmodium falciparum* sporozoite vaccine in adults during an intense malaria transmission season in Mali: a randomised, controlled phase 1 trial. *Lancet Infect. Dis.* **22**, 377–389 (2022).
20. Ocana-Morgner, C., Mota, M. M. & Rodriguez, A. Malaria blood stage suppression of liver stage immunity by dendritic cells. *J. Exp. Med.* **197**, 143–151 (2003).
21. Olsen, T. M., Stone, B. C., Chuenchob, V. & Murphy, S. C. Prime-and-trap malaria vaccination to generate protective CD8$^+$ liver-resident memory T cells. *J. Immunol.* **201**, 1984–1993 (2018).
22. Gola, A. et al. Prime and target immunization protects against liver-stage malaria in mice. *Sci. Transl. Med.* **10**, eaap9128 (2018).
23. Holz, L. E. et al. Glycolipid-peptide vaccination induces liver-resident memory CD8$^+$ T cells that protect against rodent malaria. *Sci. Immunol.* **5**, eaaz8035 (2020).
24. Brennan, P. J., Brigl, M. & Brenner, M. B. Invariant natural killer T cells: an innate activation scheme linked to diverse effector functions. *Nat. Rev. Immunol.* **13**, 101–117 (2013).
25. Heide, J., Vaughan, K. C., Sette, A., Jacobs, T. & Schulze Zur Wiesch, J. Comprehensive Review of human *Plasmodium falciparum*-specific CD8+ T cell epitopes. *Front. Immunol.* **10**, 397 (2019).
26. Morita, M. et al. Structure-activity relationship of alpha-galactosylceramides against B16-bearing mice. *J. Med. Chem.* **38**, 2176–2187 (1995).
27. Hogquist, K. A. et al. T cell receptor antagonist peptides induce positive selection. *Cell* **76**, 17–27 (1994).
28. Compton, B. J. et al. Enhancing T cell responses and tumour immunity by vaccination with peptides conjugated to a weak NKT cell agonist. *Org. Biomol. Chem.* **17**, 1225–1237 (2019).
29. Compton, B. J. et al. Synthesis and activity of 6''-deoxy-6''-thio-α-GalCer and peptide conjugates. *Org. Lett.* **17**, 5954–5957 (2015).
30. Hung, J. T. et al. Design and synthesis of galactose-6-OH-modified α-galactosyl ceramide analogues with Th2-biased immune responses. *RSC Adv.* **4**, 47341–47356 (2014).
31. Chennamadhavuni, D. et al. Dual modifications of α-galactosylceramide synergize to promote activation of human invariant natural killer T cells and stimulate anti-tumor immunity. *Cell Chem. Biol.* **25**, 571–584 (2018).
32. Christo, S. N. et al. Discrete tissue microenvironments instruct diversity in resident memory T cell function and plasticity. *Nat. Immunol.* **22**, 1140–1151 (2021).

33. Carvalho, L. H. et al. IL-4-secreting CD4$^+$ T cells are crucial to the development of CD8$^+$ T-cell responses against malaria liver stages. *Nat. Med.* **8**, 166–170 (2002).
34. Valencia-Hernandez, A. M. et al. A natural peptide antigen within the *Plasmodium* ribosomal protein RPL6 confers liver TRM cell-mediated immunity against malaria in mice. *Cell Host Microbe* **27**, 950–962 (2020).
35. Evrard, M. et al. Sphingosine 1-phosphate receptor 5 (S1PR5) regulates the peripheral retention of tissue-resident lymphocytes. *J. Exp. Med.* **219**, e20210116 (2022).
36. Grunwitz, C. et al. HPV16 RNA-LPX vaccine mediates complete regression of aggressively growing HPV-positive mouse tumors and establishes protective T cell memory. *Oncoimmunology* **8**, e1629259 (2019).
37. Salomon, N. et al. Local radiotherapy and E7 RNA-LPX vaccination show enhanced therapeutic efficacy in preclinical models of HPV16$^+$ cancer. *Cancer Immunol. Immunother.* **71**, 1975–1988 (2022).
38. Salomon, N. et al. A liposomal RNA vaccine inducing neoantigen-specific CD4$^+$ T cells augments the antitumor activity of local radiotherapy in mice. *Oncoimmunology* **9**, 1771925 (2020).
39. Sahin, U. et al. An RNA vaccine drives immunity in checkpoint-inhibitor-treated melanoma. *Nature* **585**, 107–112 (2020).
40. Kranz, L. M. et al. Systemic RNA delivery to dendritic cells exploits antiviral defence for cancer immunotherapy. *Nature* **534**, 396–401 (2016).
41. Mallory, K. L. et al. Messenger RNA expressing PfCSP induces functional, protective immune responses against malaria in mice. *NPJ Vaccines* **6**, 84 (2021).
42. Godfrey, D. I., Le Nours, J., Andrews, D. M., Uldrich, A. P. & Rossjohn, J. Unconventional T cell targets for cancer immunotherapy. *Immunity* **48**, 453–473 (2018).
43. Giaccone, G. et al. A phase I study of the natural killer T-cell ligand alpha-galactosylceramide (KRN7000) in patients with solid tumors. *Clin. Cancer Res.* **8**, 3702–3709 (2002).
44. Tefit, J. N. et al. Efficacy of ABX196, a new NKT agonist, in prophylactic human vaccination. *Vaccine* **32**, 6138–6145 (2014).
45. Guevara, M. L., Jilesen, Z., Stojdl, D. & Persano, S. Codelivery of mRNA with α-galactosylceramide using a new lipopolyplex formulation induces a strong antitumor response upon intravenous administration. *ACS Omega* **4**, 13015–13026 (2019).
46. Verbeke, R. et al. Broadening the message: a nanovaccine co-loaded with messenger RNA and α-GalCer induces antitumor immunity through conventional and natural killer T cells. *ACS Nano* **13**, 1655–1669 (2019).
47. Miyamoto, K., Miyake, S. & Yamamura, T. A synthetic glycolipid prevents autoimmune encephalomyelitis by inducing TH2 bias of natural killer T cells. *Nature* **413**, 531–534 (2001).
48. Kain, L. et al. The identification of the endogenous ligands of natural killer T cells reveals the presence of mammalian α-linked glycosylceramides. *Immunity* **41**, 543–554 (2014).
49. Schmidt, N. W. et al. Memory CD8 T cell responses exceeding a large but definable threshold provide long-term immunity to malaria. *Proc. Natl Acad. Sci. USA* **105**, 14017–14022 (2008).
50. Murphy, S. C., Kas, A., Stone, B. C. & Bevan, M. J. A T-cell response to a liver-stage *Plasmodium* antigen is not boosted by repeated sporozoite immunizations. *Proc. Natl Acad. Sci. USA* **110**, 6055–6060 (2013).
51. Wilson, N. S. et al. Systemic activation of dendritic cells by Toll-like receptor ligands or malaria infection impairs cross-presentation and antiviral immunity. *Nat. Immunol.* **7**, 165–172 (2006).

[1]Ferrier Research Institute, Victoria University of Wellington, Lower Hutt, New Zealand. [2]Maurice Wilkins Centre for Molecular Biodiscovery, Auckland, New Zealand. [3]Department of Microbiology and Immunology, The Doherty Institute for Infection and Immunity, University of Melbourne, Parkville, Victoria, Australia. [4]Malaghan Institute of Medical Research, Wellington, New Zealand. [5]Infection and Immunity Program and Department of Biochemistry and Molecular Biology, Biomedicine Discovery Institute, Monash University, Clayton, Victoria, Australia. [6]Centenary Institute and University of Sydney, AW Morrow Gastroenterology and Liver Centre, Royal Prince Alfred Hospital, Sydney, New South Wales, Australia. [7]School of BioSciences, University of Melbourne, Parkville, Victoria, Australia. [8]Department of Immunology and Infectious Disease, John Curtin School of Medical Research, Australian National University, Canberra, Australian Capital Territory, Australia. [9]Shionogi Global Infectious Diseases Division, Institute of Tropical Medicine, Nagasaki University, Sakamoto, Nagasaki, Japan. [10]Department of Biochemistry and Chemistry, La Trobe Institute for Molecular Science, La Trobe University, Bundoora, Victoria, Australia. [11]Institute of Infection and Immunity, Cardiff University School of Medicine, Cardiff, UK. [12]School of Biological Sciences, Victoria University of Wellington, Wellington, New Zealand. [13]These authors contributed equally: Mitch Ganley, Lauren E. Holz. [14]These authors jointly supervised this work: Gavin F. Painter, Ian F. Hermans, William R. Heath. ✉e-mail: gavin.painter@vuw.ac.nz; ihermans@malaghan.org.nz; wrheath@unimelb.edu.au

Methods

Experimental work (vaccination, tissue processing, flow cytometry and sporozoite challenges) corresponding to Figs. 1, 3a–c and 5–8 was performed at the University of Melbourne, whereas the work (vaccination, tissue processing and flow cytometry) corresponding to Figs. 2, 3d–h and 4 was performed at the Malaghan Institute of Medical Research.

Mice

Mice were sex matched and used between 6 and 12 weeks of age, and were from either the Bioresources Facility at the Department of Microbiology and Immunology, The University of Melbourne, Australia, or the Biomedical Research Unit at the Malaghan Institute of Medical Research, New Zealand. Experiments were carried out under pathogen-free conditions, with mice kept at 20–26 °C, 45–65% humidity and a 12-h day–night light cycle. Animals used for the generation of the sporozoites were 4–5-week-old male Swiss Webster mice purchased from Monash Animal Services (Melbourne, Victoria, Australia) and maintained at the School of Botany, The University of Melbourne, Australia. Vaccine studies used C57BL/6J mice (B6) (Jackson Laboratories); *Traj18*$^{-/-}$ mice, which are devoid of type I NKT cells[52] (Jackson Laboratories); *Cd40*$^{-/-}$ mice, which lack expression of CD40 (ref. 53); *Batf3*$^{-/-}$ mice, which lack cDC1 (ref. 54); Ly5.1^{+} *Il15*$^{-/-}$ mice, which lack expression of IL-15 (ref. 55); IA$^{-/-}$ mice, which lack all IA and IE genes[56]; and OT-I mice, which express a transgenic TCR that recognizes residues 257–264 of the model antigen chicken OVA[27]; these mice were maintained on a B6.SJL background (CD45.1^{+}).

Ethics

All animal experiments were in accordance with the Prevention of Cruelty to Animals Act 1986, the Prevention of Cruelty to Animals Regulations 2008, the National Health and Medical Research Council (2013) Australian code for the care and use of animals for scientific purposes, or the Animal Welfare Act of New Zealand (1999). The protocols were approved by the Melbourne Health Research Animal Ethics Committee, University of Melbourne (ethics protocols: 1714302, 1914923) or by the Victoria University of Wellington Animal Ethics Committee (AEC23784 and AEC26384)

Adoptive transfer of OT-I.CD45.1 cells

For the experiments corresponding to Figs. 1, 3a–c and 8, naive OT-I CD8 T cells were enriched from spleens by negative selection. The tissue was first teased through a 70-µm filter, and the cell suspension was incubated in RBC lysis solution at 20–22 °C for 5 min, before being washed with RPMI and incubated in 1 ml of a cocktail containing rat anti-mouse antibodies (anti-Ly-76, clone TER119; anti-MHC II, clone M5-114; anti-CD4, clone GK1.5; anti-Gr-1, clone RB6-8C5; anti-Mac-1, clone M1/70; clone F4/80) for 30 min on ice. After a further wash, the cells were incubated with goat anti-rat IgG magnetic beads (QIAGEN, 1:10 cell/bead ratio) for 20 min on a roller at 4 °C. The tube was then placed near a magnet to retain bead-bound cells, and the supernatant containing unbound cells was collected. Enriched naive CD8 T cells were counted, and their purity was analyzed by staining with anti-CD8α and anti-Vα2 TCR antibodies. Cell counts were adjusted to 2.5×10^5 cells per ml in phosphate-buffered saline (PBS), and mice were injected i.v. with 200 µl of cell suspension. For the experiments corresponding to Figs. 2, 3d,g and 4, naive OT-I CD8 T cells were pooled from lymph nodes that had been teased through a 70-µm filter, washed and resuspended in Iscove's modified Dulbecco's medium (IMDM; Gibco). The proportion of naive (CD8^{+} CD44^{lo} CD62L^{hi}) CD8 T cells (OT-I cells) was established by flow cytometry, with 5×10^4 OT-I cells injected i.v. into each host.

Vaccine preparation

Genes for OVA (NP_990483) and the malaria antigen RPL6 (PBANKA_135190)[8] were codon-optimized for mammalian expression based on the most abundant transfer RNAs using bioinformatics software Geneious Prime 2023.1.2 (Biomatters Ltd.). A consensus Kozak sequence/start codon and two stop codons after the gene of interest were included in the sequence. DNA for both genes was synthesized by Twist Bioscience and cloned into pVAX1 (Thermo Fisher Scientific) containing a T7 RNA polymerase promoter, with restriction enzymes EcoRI/NotI and BamHI/EcoRI (New England Biolabs), respectively. NotI enzyme (New England Biolabs) was used for template linearization before purification with silica chromatography using a DNA Clean and Concentrator-5 kit (Zymo Research), and in vitro transcription was conducted using a HiScribe T7 High Yield RNA Synthesis Kit (New England Biolabs). DNase I (New England Biolabs) was used to remove template DNA before precipitation of the RNA product using 2 M LiCl, followed by incubation at −20 °C for 30 min and centrifugation at 16,000g for 20 min at 4 °C. A m^{7}GpppG mRNA cap was added to the RNA using the Vaccinia Capping System (New England Biolabs), and a polyA tail was added with an *Escherichia coli* polyA polymerase (New England Biolabs). RNA integrity and polyA tail length (~200 bp) were confirmed using agarose gel electrophoresis and RNA ScreenTape analysis with an Agilent 4200 TapeStation (Agilent Technologies Ltd.). For preparation of lipoplex mRNA vaccines, liposomes were first produced using an adaption of the thin-film hydration method[40]. Briefly, the appropriate amount of a 3:1 molar ratio of DOTMA [1,2-di-O-octadecenyl-3-trimethylammonium propane (chloride salt)] and DOPE [dioleoyl phosphatidylethanolamine] (Avanti Lipids) was dissolved in ethanol or chloroform and transferred to a round-bottomed flask or test tube. The appropriate adjuvants were added to 0.06 mol.% of the total lipid amount (for the standard 80 pmol dose) as a solution in ethanol or hexafluoroisopropanol. For dose titration, the amount of adjuvant was reduced to 0.006% (8 pmol dose) and 0.0006% (0.8 pmol dose). Solvent was removed under vacuum or a stream of argon gas and further dried under vacuum. The resulting thin film was hydrated with UltraPure DNase/RNase-Free distilled water (Thermo Fisher Scientific) by overnight incubation at 4 °C to a final lipid concentration of 6 mM. The material was then sonicated and extruded with 11 passes through a 200 nm polycarbonate membrane using a Mini-Extruder (Avanti Lipids) or 200-nm NanoSizer MINI Liposome Extruder (T&T Scientific Corp.). For preparation of lipoplexes, RNA (1 mg ml^{-1}) in 100 mM HEPES-buffered solution (pH 7.2–7.5) with 1.5 M NaCl was complexed with liposomes using a lipid-to-mRNA phosphate molar ratio of 9:1, to a final concentration of 10 mM HEPES, 150 mM NaCl. Lipoplex size was determined by dynamic light scattering using a Malvern Zetasizer Nano ZS (Malvern Panalytical). Lipoplexes were typically 260 nm in size (Z average) with a polydispersity index of 0.2 and zeta potential of 60 mV. The lipoplex–mRNA vaccine was diluted two-fold in PBS (Thermo Fisher Scientific) before i.v. injection in the tail vein.

NKT agonist preparation

The NKT cell agonists αGC, αGC_N and αGC_S were synthesized as reported previously[57]. Briefly, an *N*-Boc and acetonide-protected α-galactosylphytosphingosine intermediate was treated with 40% trifluoroacetic acid in dichloromethane to give α-galactosylphytosphingosine, which was in turn reacted with an activated form of cerotic acid to give αGC. Alternatively, the protected α-galactosylphytosphingosine intermediate was reacted with triisopropylbenzenesulfonyl chloride to selectively protect the *O*-6 position of the galactose moiety. Subsequent per-*O*-acetylation gave a substrate suitable for installing the required *S*- or *N*-heteroatoms at position 6 of the galactose ring. For αGC_N, the sulfonate intermediate was treated with sodium azide, followed by removal of the protecting groups to afford 6′-azido-6′-deoxy-α-galactosylphytosphingosine; this was *N*-acylated with cerotic acid, followed by H_2/Pd-mediated azide reduction. αGC_S was formed by treating the sulfonate with potassium thioacetate, followed by global deprotection. The resulting thiol was protected as a pyridyl disulfide, allowing *N*-acylation with cerotic acid. TCEP-mediated disulfide reduction afforded αGC_S. αGC_B was

synthesized according to published procedures[28], whereby αGC_S was reacted with 1,3,5,7-tetramethyl-8-phenyl(4-iodoacetamido)-difluoroboradiaza-s-indacene and *N*,*N*-diisopropylethylamine in a 1:1 mixture of dry dimethylformamide and chloroform.

mRNA vaccination

For all experiments, mice were injected i.v. with 5 µg mRNA in the relevant mRNA vaccine in 200 µl PBS.

In vivo antibody-mediated inhibition

Anti-CD40L (CD154) (clone MR-1) or polyclonal Armenian hamster IgG (BioXCell) (0.5 mg) was administered intraperitoneally (i.p.) on day −1 and day 0 of vaccination. Anti-IFNαR1 (clone MAR1-5A3) or mouse IgG1 (clone MOPC-21) isotype control (BioXCell) (1.2 mg) was administered i.p. 4 h before vaccination (day 0) and on days 1 and 3. Anti-IL-4 (clone 11B11) or mouse IgG1 anti-HRP (clone HRPN) isotype control (BioXCell) (0.5 mg) was administered i.p. 4 h before vaccination (day 0) and on days 1 and 3. Anti-IL-12p35 (clone C18.2), anti-IL-15 (clone AIO.3), anti-GM-CSF (clone MP1-22E9), anti-IFNγR1 (clone GR-20) or mouse IgG2a anti-trinitrophenol (clone 2A3) isotype control (BioXCell) (0.5 mg) was administered i.p. 4 h before vaccination (day 0) and on days 1 and 3.

Mosquitoes and sporozoite challenge

Anopheles stephensi mosquitoes (strain STE2/MRA-128 from BEI Resources, The Malaria Research and Reference Reagent Resource Center) were reared as described previously[58]. *A. stephensi* mosquitoes (STE2, MRA-128, from BEI Resources) were reared in an insectary approved by the Australian Department of Agriculture, Fisheries and Forestry, which was maintained at 27 °C and 75–80% humidity on a 12-h light–dark cycle. The larvae were bred in plastic food trays (P.O.S.M. Pty Ltd.) containing 300 larvae in filtered drinking water (Frantelle beverages) changed every 3 days and fed with Sera vipan baby fish food (Sera). Upon ecloding, adult mosquitoes were transferred to aluminum cages (BioQuip Products, Inc.) and kept in a secure incubator (Conviron) in the insectary at the same temperature and humidity, maintained on 10% sucrose. The *Plasmodium* species used to raise infectious mosquitoes were PbA wild-type Cl15cy1 (BEI Resources, NIAID, NIH: MRA-871) and PbA-expressing OVA under the HSP70 promoter[59]. Naive Swiss mice were inoculated i.p. with infected RBC from an infected syngeneic donor, with parasitemia then confirmed by Giemsa smear and exflagellation quantified 3 days postinfection. Adult *A. stephensi* mosquitoes were then allowed to feed on anaesthetized mice, and 22 days later sporozoites were dissected from mosquito salivary glands and resuspended in cold PBS. For challenge experiments, 200 freshly dissected sporozoites were i.v. injected. Blood samples were assessed for parasitemia on days 6, 7, 8, 10 and 12 by flow cytometry after staining with Hoechst 33258 dye (Thermo Fisher) for 1 h at 37 °C. An LSR Fortessa (BD Biosciences) with a violet laser (405 nm) was used to excite the dye in infected RBC, and percentages of Hoechst-positive cells were compared with those from uninfected controls. Values of >0.1% were considered to indicate positivity for parasites, and mice positive for two consecutive days were euthanized. Those remaining parasitemia-negative on day 12 were considered to be protected[23].

RAS vaccination

CS^{5M} OVA-expressing sporozoites[60] (5×10^4) were irradiated with 20,000 rads using a gamma ^{60}Co source and then i.v. injected into recipient mice[8].

Exposure to *P. chabaudi* blood stage and curing

Donor B6 mice were injected with frozen stabilates of blood-stage *P. chabaudi* parasites. Three to seven days later, the mice were bled, their parasitemia was measured, and recipient mice were injected i.p. with 50,000 *P. chabaudi*-infected RBC diluted in 0.2 ml PBS. For curing of infections, mice were injected i.p. with 0.8 mg chloroquine for 5 consecutive days, starting at day 30, followed by provision of drinking water containing 600 mg l^{-1} chloroquine from the day of last i.p. injection for 3 days.

Immune cell depletion in vivo

For depletion of T cell subsets, B6 mice were treated i.v. with 250 µg anti-CXCR3 (clone CXCR3-173), anti-mouse Ly6G/Ly6C [(Gr-1) NIMP-R14], or Isotype Rat IgG2b, κ (BioXCell) and polyclonal Armenian hamster IgG at the indicated time points as previously described[8,32]. Depletion of cells was assessed 5 days later by flow cytometry. For depletion of CD8 cells, mice were injected i.v. with 100 µg anti-CD8 antibody (clone 2.43) or isotype control (GL117, IgG2a) 1 day before challenge. For depletion of CD4 T cells, NK cells and NKT cells, mice were injected with two doses of 100 µg anti-CD4 (clone GK1.5) or isotype control (IgG2b κ) on days 6 and 2 before challenge and three doses of 100 µg anti-NK1.1 (clone PK136) or isotype control (IgG2a k) on days 3, 2 and 1 before challenge, as previously described[8].

Splenectomy

For splenectomy, mice were anesthetized by isoflurane inhalation (3% for induction, 1.5–2.0% for maintenance), with 0.1 mg kg^{-1} buprenorphine given via subcutaneous injection for analgesia (Sigma-Aldrich). Lacrilube (Allergan) was applied to corneas to prevent desiccation. The surgical area was sterilized with iodine, and then an incision was made on the left flank and peritoneum to access the spleen. The primary artery and vein were tied using sutures (Ethicon Prolene 7/0 Blue P1 45 cm, Amtech), the spleen was removed, and the incision was closed by suture. Sham surgeries were performed where the peritoneum was cut and then closed by suture. Postoperative analgesia with 5 mg kg^{-1} carprofen (Norbrook Laboratories) was given subcutaneously for 2 days after surgery.

Tissue processing for flow cytometry

Blood was either collected from the tail veins of mice in tubes containing 10 U heparin (Fig. 1) or collected from the submandibular vein punctured with a 4-nm Goldenrod Animal Lancet and collected into 200 µl 10 mM EDTA/PBS (Fig. 4). Tubes were centrifuged at 1503*g* for 4 min, and cells were resuspended in 1 ml RBC lysis solution (QIAGEN). After 20 min at 37 °C, leukocytes were harvested by centrifugation and resuspended in 200 µl FACS buffer (PBS with 5 mM EDTA, 2.5% bovine serum albumin) for antibody staining in a 96-well plate.

Livers were collected into tubes containing RPMI, 2% fetal calf serum (FCS) and 10 U heparin. Each liver was teased through a 70-µm cell strainer and washed with RPMI, and the cell suspension was resuspended in 30 ml 35% Percoll (GE Healthcare) before centrifugation at 500*g* for 20 min at 20–22 °C, with no brake. The cell pellet was incubated in 5 ml RBC lysis solution for 5 min at 20–22 °C before being washed with 30 ml RPMI and resuspended in 1 ml of FACS buffer for flow cytometry. One-fifth of the cell suspension was used for antibody staining. Spleen lymphocytes were isolated by teasing tissue through a 70-µm strainer, washing in RPMI, 2% FCS, incubating cells in RBC lysis solution for 1–2 min at 20–22 °C, washing again and resuspending in 5 ml FACS buffer. Approximately 1/25 of the final volume was used for antibody staining. Lung tissue was incubated for 45 min at 37 °C in 0.1 mg ml^{-1} Liberase TL (Roche) and 0.2 mg ml^{-1} DNase I (Roche) in 1 ml RPMI, before 50 µl of EDTA (0.5 M solution) was added for a further 5 min. Each lung sample was passed through a 3-ml syringe, teased through 70-µm mesh, incubated in 2 ml RBC lysis solution for 10 min at 20–22 °C and resuspended in 1 ml FACS buffer; 1/10 of the final volume was used for antibody staining.

For the assessment of splenic dendritic cells (DC) by flow cytometry, spleens were injected at 4–5 points with 0.5 ml IMDM supplemented with 0.3 mg ml^{-1} Liberase TL and 0.2 mg ml^{-1} DNase 1, digested in this mix for 30 min at 37 °C and then mechanically dissociated through a

70-µm sieve with 20 ml IMDM. Samples were centrifuged at 572*g* for 4 min, supernatants were discarded, and pellets were resuspended in 2 ml RBC lysis buffer. Samples were centrifuged and resuspended in 1 ml FACS buffer, and 100 µl was transferred to a 96-well plate for staining.

Tissue was prepared for assessment of liver DC populations as previously decribed[61]. Briefly, livers were perfused with collagenase type IV (Sigma) and then digested in collagenase for 45 min at 37 °C. Cell suspensions were passed through 70-µm sieves, washed with PBS and resuspended in a 33% Percoll solution (Sigma). Samples were centrifuged at 693*g* for 12 min, with no brake. RBC were removed using lysis buffer, and one-fifth of isolated cells were stained for flow cytometry analysis.

K^b-$RPL6_{120–127}$ production

The H2-K^b (K^b) heavy chain (1-275) with a BirA tag for biotinylation was produced in *E. coli* cells, as well as the human β2 microglobulin (β2m) as per a previously described method[62]. The K^b-$RPL6_{120–127}$ complex was then refolded with 30 mg of heavy chain, 10 mg of β2m and 4 mg of the $RPL6_{120–127}$ peptide[62]. The final protein was purified and biotinylated before tetramerization.

Antibody staining and flow cytometry

Antibody panels used for staining were optimized elsewhere[63] and are provided in Supplementary Table 1. Methods for flow cytometry of T cells in liver, spleen and lung samples have been described elsewhere[63]. For the experiments corresponding to Figs. 5–7, lymphocytes were stained with K^b-$RPL6_{120–127}$-specific tetramers for 1 h at 20–22 °C before staining with surface antibodies. For experiments corresponding to Fig. 4, lymphocytes were stained with K^b-$OVA_{257–264}$-specific pentamers at optimal concentrations for the tissue type (1 µl for blood, 2 µl for spleen and lung, and 3 µl for liver, in 10 µl FACS buffer) for 15 min at 20–22 °C before staining with surface antibodies. Flow cytometry data were collected on an Aurora (Cytek) cytometer using SpectroFlo v.3 software (Cytek) or an LSRFortessa cytometer (BD Biosciences) using FACSDiva v.9 software (BD Biosciences). Flow cytometry data were analyzed using FlowJo v.9 and v.10 (Treestar).

Production of mouse CD1d and the 2C12 TCR

The recombinant mCD1d was expressed in Hi5 insect cells using the baculovirus expression system and purified by nickel-affinity and size exclusion chromatography techniques as previously described[31]. The 2C12 TCRα and TCRβ chains were expressed in *E. coli* and purified as inclusion bodies, and the 2C12 TCR heterodimer was in vitro refolded and purified as previously described[31].

Loading of αGC_B into CD1d

αGC_B was dissolved in 0.5% tyloxapol at 1 mg ml^{-1}. The solution was then sonicated for 30 min and immediately transferred to a 60 °C water bath for 1 min and left to cool at 20–22 °C for 1 min. αGC_B was then added directly to mCD1d at a 6:1 molar ratio and incubated in 10 ml TBS150 (Tris-buffered saline, 150 mM NaCl, 10 mM Tris pH 8.0) at 20–22 °C for 15 h. The mCD1d–αGC_B binary complex was then purified using size exclusion chromatography.

Affinity measurements of the 2C12 TCR against mCD1d–αGC_B

The affinity between the 2C12 TCR and mCD1d loaded with αGC_B was measured by surface plasmon resonance using a Biacore3000 (GE Healthcare). mCD1d–αGC_B was biotinylated and passed over a streptavidin-coated chip in HEPES-buffered saline (150 mM NaCl, 10 mM HEPES, pH 7.4 and 0.5% bovine serum albumin) until 3000 response units of biotinylated mCD1d–αGC_B had been captured on the chip surface. A series of 12 two-fold dilutions of the 2C12 TCR ranging from 4.5 nM to 5 µM in HBS buffer at 25 °C was used to examine the affinity for mCD1d–αGC_B. The TCR was passed over the streptavidin-coated chip for 120 s at a flow rate of 5 µl min^{-1}. BIAevaluation 3.1 software (Biacore AB) was used to estimate steady-state K_d values, and GraphPad Prism 9 was used for statistical analysis, curve fitting and graphic presentation.

Serum IL-4 detection

Blood was collected in Microvette 500 Z-Gel tubes (Sarstedt) and centrifuged for 5 min at 10,000*g* to produce serum. Levels of IL-4 were measured using the BioPlex Pro Mouse Cytokine 23-plex assay (Bio-Rad).

Serum anti-OVA IgG enzyme-linked immunosorbent assay

Nunc-Immuno MicroWell 96-well solid plates (Sigma) were coated with 20 µg ml^{-1} EndoGrade OVA (Lionex Therapeutics and Diagnostics) in 0.1 M sodium carbonate buffer overnight at 4 °C. After blocking with 10% FCS for 1 h at 20–22 °C, eight ten-fold dilutions (10^{-2} to 10^{-9}) of each sample were added to the plates, followed by incubation for 2 h at 20–22 °C. Plate-bound IgG was detected using 1:1000 dilution goat anti-mouse IgG HRP conjugate (Thermo Fisher Scientific) for 1 h at 20–22 °C. Plates were developed with a BD OptEIA TMB Substrate Reagent Set (BD Biosciences) and 2 M H_2SO_4 stop solution. Absorbance maximum at 450 nm was used for enzyme-linked immunosorbent assay plate readings.

Statistics

Treatments were assigned to separately caged litter groups. No statistical methods were used to predetermine sample sizes, but our sample sizes were similar to those reported in previous publications[8,23]. Numerical data from FlowJo were exported to Excel 16.73 (Microsoft) for calculations of cell counts and percentages. Data are shown as mean values ± s.e.m., and plots of individual data points (individual mice) are provided for all experiments to show distribution. Data analyzed included outliers unless these could be explained by technical error. Data collection and analysis were not performed blind to the conditions of the experiments. Data were assumed to be normal, but this was not formally tested because the sample sizes used were not well powered for normality testing. The statistical tests performed on the data are indicated in the figure legends, along with sample sizes. Individual *P* values are provided in the figures; ****$P < 0.0001$. Prism v.9 (GraphPad) was used for statistical tests and graphs.

Reporting summary

Further information on research design is available in the Nature Portfolio Reporting Summary linked to this article.

Data availability

Data to support the findings of study are available from the corresponding author upon request without restrictions. Source data are provided with this paper.

References

52. Chandra, S. et al. A new mouse strain for the analysis of invariant NKT cell function. *Nat. Immunol.* **16**, 799–800 (2015).
53. Kawabe, T. et al. The immune responses in CD40-deficient mice: impaired immunoglobulin class switching and germinal center formation. *Immunity* **1**, 167–178 (1994).
54. Hildner, K. et al. Batf3 deficiency reveals a critical role for CD8alpha$^+$ dendritic cells in cytotoxic T cell immunity. *Science* **322**, 1097–1100 (2008).
55. Kennedy, M. K. et al. Reversible defects in natural killer and memory CD8 T cell lineages in interleukin 15-deficient mice. *J. Exp. Med.* **191**, 771–780 (2000).
56. Madsen, L. et al. Mice lacking all conventional MHC class II genes. *Proc. Natl Acad. Sci. USA* **96**, 10338–10343 (1999).
57. Meijlink, M. A. et al. 6′′-modifed α-GalCer-peptide conjugate vaccine candidates protect against liver-stage malaria. *RSC Chem. Biol.* **3**, 551–560 (2022).

58. Benedict, M. Q. in *The Molecular Biology of Insect Disease Vectors* (eds Crampton, J. M. et al.) Ch. 1 (Chapman & Hall, 1997).
59. Kimura, K. et al. CD8$^+$ T cells specific for a malaria cytoplasmic antigen form clusters around infected hepatocytes and are protective at the liver stage of infection. *Infect. Immun.* **81**, 3825–3834 (2013).
60. Cockburn, I. A. et al. Dendritic cells and hepatocytes use distinct pathways to process protective antigen from *Plasmodium* in vivo. *PLoS Pathog.* **7**, e1001318 (2011).
61. Beattie, L. et al. A transcriptomic network identified in uninfected macrophages responding to inflammation controls intracellular pathogen survival. *Cell Host Microbe* **14**, 357–368 (2013).
62. Chatzileontiadou, D. S. M., Szeto, C., Jayasinghe, D. & Gras, S. Protein purification and crystallization of HLA-A∗02:01 in complex with SARS-CoV-2 peptides. *STAR Protoc.* **2**, 100635 (2021).
63. Farrand, K. et al. Using full-spectrum flow cytometry to phenotype memory T and NKT cell subsets with optimized tissue-specific preparation protocols. *Curr. Protoc.* **2**, e482 (2022).

Acknowledgements

We thank the BRF at the Peter Doherty Institute, and the BRU and the Hugh Green Cytometry Centre at the Malaghan Institute of Medical Research for technical support. We thank D. Bowen for support of K.E., D. Godfrey for the CD1d–PBS-44 tetramers and the NIH tetramer core facility for the CD1d–PBS-57 tetramers. This work was supported by funding from the New Zealand Ministry of Business Innovation and Employment (contract RTVU1603 to Victoria University of Wellington) and the New Zealand Health Research Council (contract HRC-20/569 to Victoria University of Wellington and HRC14/1003 Independent Research Organisation Fund to the Malaghan Institute). K.C.Y.P. is supported by the Monash Graduate Scholarship and the Monash University MNHS Faculty International Tuition Scholarship. D.F.R. was supported by the National Health and Medical Research Council of Australia (NHMRC) 1139486, S.G. by NHMRC 1159272, P.B. and K.E. by NHMRC 1146677, W.R.H. by NHMRC 1154457, and W.R.H. and L.E.H. by NHMRC 2012701.

Author contributions

W.R.H., I.F.H, G.F.P, D.F.-R., L.E.H., D.F.A. and M.G. conceived the idea and designed the outline of the research. A.C., I.A.C., K.Y. and G.I.M. provided sporozoites for infection studies. K.C.Y.P., J.L.N. and J.R. carried out affinity measurements of 2C12 TCR–CD1d–αGC_B by surface plasmon resonance. W.R.H., I.F.H., G.F.P., L.E.H. and M.G. wrote the manuscript. J.L.N., S.L.D., S.T.S.C, R.J.A., B.J.C. A.J.M. O.K.B. and J.J.M. wrote Methods sections. All authors contributed to reviewing and editing the manuscript and to relevant discussions. M.G., K.J.F., O.K.B., J.C.M., M.M., L.E.H., J.J.M., Y.C.C. and Z.G. vaccinated mice, analyzed T cell responses and examined protection. S.L.D., M.G., J.J.M., S.T.S.C, R.J.A., B.J.C. and A.M. prepared vaccines and vaccine components. S.G. produced K^b tetramers. C.X. produced CD1d–PBS-44 tetramers. K.E. and P.B. contributed to analysis of liver DC.

Competing interests

M.G., L.E.H., R.J.A., B.J.C., A.J.M. I.F.H., W.R.H. and G.F.P. are inventors on a patent application (WO2023121483A1) submitted by Victoria University of Wellington subsidiary Victoria Link Limited that covers the production of tissue-resident memory T cells with mRNA vaccines.

Additional information

Extended data is available for this paper at https://doi.org/10.1038/s41590-023-01562-6.

Supplementary information The online version contains supplementary material available at https://doi.org/10.1038/s41590-023-01562-6.

Correspondence and requests for materials should be addressed to Gavin F. Painter, Ian F. Hermans or William R. Heath.

Peer review information *Nature Immunology* thanks Rafick Sekaly and the other, anonymous, reviewer(s) for their contribution to the peer review of this work. Primary Handling Editor: Jamie D. K. Wilson, in collaboration with the *Nature Immunology* team.

https://doi.org/10.1038/s41590-023-01562-6

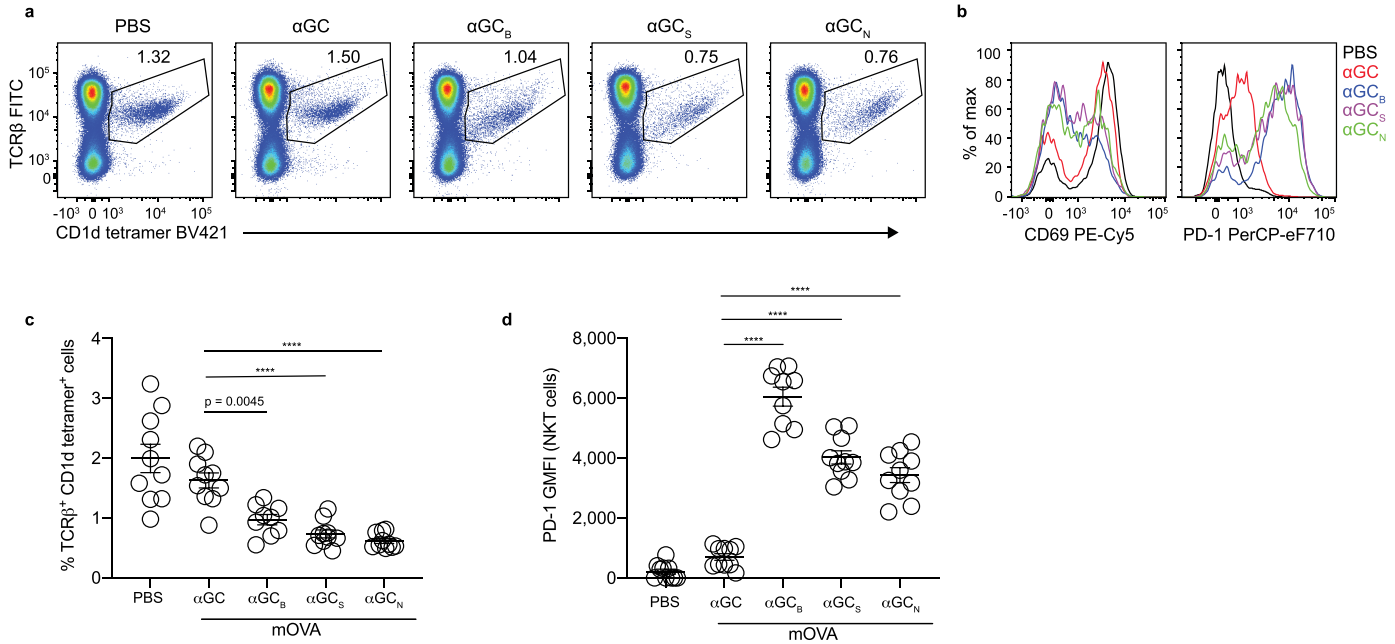

Extended Data Fig. 1 | Vaccine-induced activation of splenic NKT cells. Male B6 mice were transferred OT-I.CD45.1 cells one day before vaccination with mOVA vaccine alone, or mOVA with 80 pmol of indicated adjuvants. Data are combined from two independent experiments, giving n = 10 mice per group with the exception of the mOVA + αGC_B group which contains 9 mice. **a**, Example flow cytometry plots showing expression of the TCR on splenic NKT cells at day 28. Gating shown in Supplementary data Fig. 4. **b**, Examples of CD69 (left) and PD-1 (right) expression on splenic NKT cells. **c**, Percentage TCRβ$^+$ CD1d-tetramer$^+$ spleen cells as gated in (a). Data are displayed as mean ± s.e.m. and individual mice (circles) and compared to the mOVA + αGC group by one-way ANOVA analysis with Tukey's multiple comparison post-test. **d**, Geometric mean fluorescence intensity of PD-1 on NKT cells. Data are displayed as mean ± s.e.m. from two independent experiments and compared to the mOVA + αGC group by one-way ANOVA analysis with Tukey's multiple comparison post-test. ****$P < 0.0001$.

https://doi.org/10.1038/s41590-023-01562-6

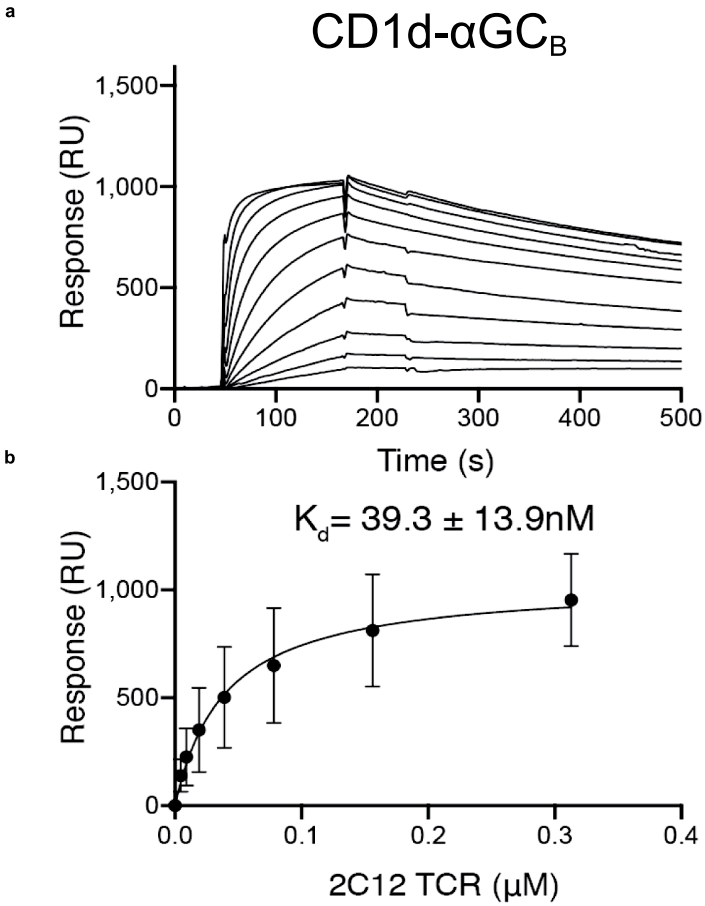

Extended Data Fig. 2 | Type I NKT 2C12 TCR binding affinity for mouse CD1d-αGC$_B$. Affinity measurement of soluble mouse type I NKT 2C12 TCR to mCD1d-αGC$_B$ using surface plasmon resonance (SPR). **a**, Equilibrium curves representative of one experiment performed in duplicate. **b**, K_d values are derived from duplicate runs from n = 3 independent experiments. Error bars on lower graph show mean ± SD.

https://doi.org/10.1038/s41590-023-01562-6

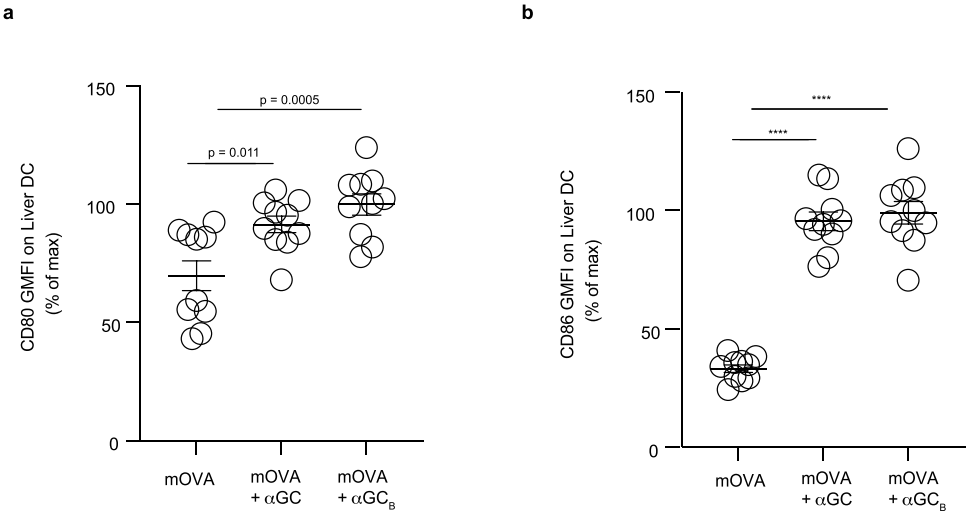

Extended Data Fig. 3 | Effect of vaccination on expression of costimulatory molecules on liver DC. Female B6 mice were vaccinated with mOVA vaccine alone or mOVA with adjuvants αGC or αGC$_B$. Livers were harvested 24 h later and DC (CD11c$^+$ MHC II$^+$ cells) assessed for relative expression of CD80 (**a**) and CD86 (**b**). Data are expressed as percent of maximum (% of max) determined by dividing the GMFI of each sample by the maximum mean GMFI of the highest mean of all groups from each experiment. Each circle depicts the values of an individual mouse (n = 10 biologically distinct samples combined from two independent experiments). Lines show mean ± s.e.m. Data (a, b) were compared by a one-way ANOVA with Tukey's multiple comparison post-test (a, b). ****$P < 0.0001$.

https://doi.org/10.1038/s41590-023-01562-6

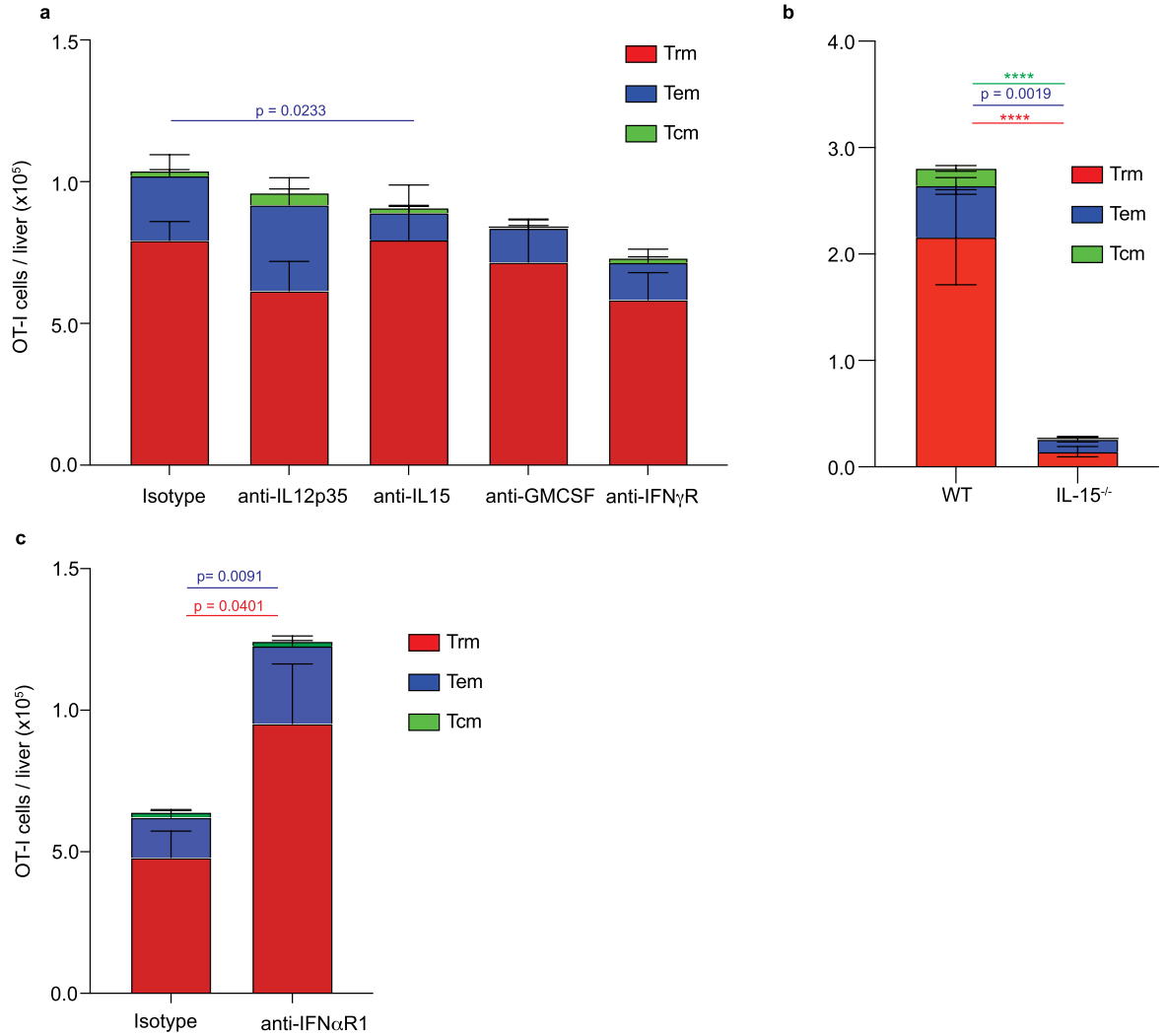

Extended Data Fig. 4 | The role of cytokines in responses to mRNA vaccination. a, Male B6 mice were transferred OT-I.CD45.1 cells one day before vaccination with mOVA + αGC_B. Groups of these mice were injected with mAb specific for blocking either IL-12p35, IL-15, GM-CSF or IFN-γR1, or with an isotype control mAb on days 0, 1 and 3 and then left to day 30 before OT-I memory T cell subsets were quantified in the liver. Gating parameters for OT-I cells are described in Supplementary data Fig. 1. Data are expressed as mean cell count ± s.e.m. for each subset. Individual values for each mouse are shown in Supplementary Fig. 8a. **b**, Female B6 mice or IL-$15^{-/-}$ mice were transferred OT-I.CD45.1 cells one day before vaccination with mOVA + αGC_B., and 36 days later OT-I memory T cell subsets were quantified in the liver. Mean cell count ± s.e.m. for each subset shown. Individual values for each mouse are shown in Supplementary Fig. 8b. **c**, Male B6 mice were OT-I.CD45.1 cells one day before vaccination mOVA + αGC_B. Groups of these mice were injected with specific mAb for blocking IFNαR1 or an isotype control on days 0, 1 and 3 and then left to day 30 before OT-I memory T cell subsets were quantified in the liver. Mean cell count ± s.e.m. for each subset shown. Individual values for each mouse are shown in Supplementary data 8c. Data in **a** were log-transformed and compared to the isotype group by one-way ANOVA with Tukey's multiple comparison post-test. Data in **b** and **c** were log-transformed and compared by two-sided unpaired Student's t tests. Two independent experiments were performed for each panel (a,b, n = 10 mice per group; c, n = 7 mice per group). ****$P < 0.0001$. Bars indicating significance are coloured to correspond to each memory T cell subset.

https://doi.org/10.1038/s41590-023-01562-6

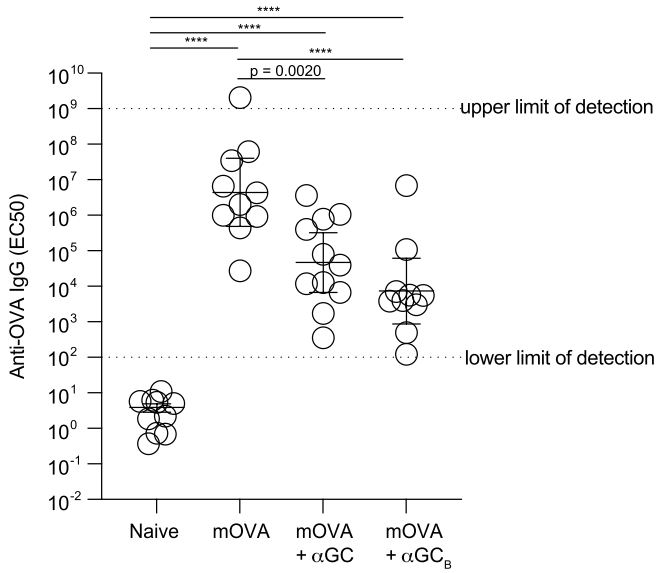

Extended Data Fig. 5 | Assessment of total anti-OVA IgG in sera 3 weeks following a prime-boost schedule. Male B6 mice were vaccinated with mOVA vaccine alone (containing 5 µg mRNA), or mOVA adjuvanted with αGC or αGC$_B$, on days 0 and 21, with sera collected 3 weeks after the boost analysed for total anti-OVA IgG by ELISA. Two independent experiments were combined to give 10 mice per group with the exception of the αGC group which contains 11 mice. Geometric mean ± 95 % confidence intervals for EC_{50} values are shown. Data were log-transformed and compared by one-way ANOVA with Tukey's multiple comparison post-test. ****$P < 0.0001$.

nature portfolio

Corresponding author(s): William R. Heath

Last updated by author(s): Jun 12, 2023

Reporting Summary

Nature Portfolio wishes to improve the reproducibility of the work that we publish. This form provides structure for consistency and transparency in reporting. For further information on Nature Portfolio policies, see our Editorial Policies and the Editorial Policy Checklist.

Statistics

For all statistical analyses, confirm that the following items are present in the figure legend, table legend, main text, or Methods section.

n/a	Confirmed	
☐	☒	The exact sample size (*n*) for each experimental group/condition, given as a discrete number and unit of measurement
☐	☒	A statement on whether measurements were taken from distinct samples or whether the same sample was measured repeatedly
☐	☒	The statistical test(s) used AND whether they are one- or two-sided *Only common tests should be described solely by name; describe more complex techniques in the Methods section.*
☒	☐	A description of all covariates tested
☐	☒	A description of any assumptions or corrections, such as tests of normality and adjustment for multiple comparisons
☐	☒	A full description of the statistical parameters including central tendency (e.g. means) or other basic estimates (e.g. regression coefficient) AND variation (e.g. standard deviation) or associated estimates of uncertainty (e.g. confidence intervals)
☐	☒	For null hypothesis testing, the test statistic (e.g. *F*, *t*, *r*) with confidence intervals, effect sizes, degrees of freedom and *P* value noted *Give P values as exact values whenever suitable.*
☒	☐	For Bayesian analysis, information on the choice of priors and Markov chain Monte Carlo settings
☒	☐	For hierarchical and complex designs, identification of the appropriate level for tests and full reporting of outcomes
☒	☐	Estimates of effect sizes (e.g. Cohen's *d*, Pearson's *r*), indicating how they were calculated

Our web collection on statistics for biologists contains articles on many of the points above.

Software and code

Policy information about availability of computer code

Data collection	For flow cytometry, samples were acquired with FACSDiva v9 software with a LSR fortessa (BD Biosciences) or Spectroflo v3 software (Cytek) with an Aurora (Cytek). Geneious Prime 2023.1.2 software was used for codon-optimization and Prism v9 software was used for statistical analysis and to create graphs.
Data analysis	Flow cytometry data was analyzed using FlowJo v9 and v10 software (Treestar). Numerical data was exported to Microsoft Excel v16.73 for further analysis. Prism v9 software (GraphPad) was used for statistical analysis and graphs.

For manuscripts utilizing custom algorithms or software that are central to the research but not yet described in published literature, software must be made available to editors and reviewers. We strongly encourage code deposition in a community repository (e.g. GitHub). See the Nature Portfolio guidelines for submitting code & software for further information.

Data

Policy information about availability of data

All manuscripts must include a data availability statement. This statement should provide the following information, where applicable:

- Accession codes, unique identifiers, or web links for publicly available datasets
- A description of any restrictions on data availability
- For clinical datasets or third party data, please ensure that the statement adheres to our policy

The data that support the findings of this study are available from the corresponding author upon reasonable request

Research involving human participants, their data, or biological material

Policy information about studies with human participants or human data. See also policy information about sex, gender (identity/presentation), and sexual orientation and race, ethnicity and racism.

Reporting on sex and gender	N/A
Reporting on race, ethnicity, or other socially relevant groupings	N/A
Population characteristics	N/A
Recruitment	N/A
Ethics oversight	N/A

Note that full information on the approval of the study protocol must also be provided in the manuscript.

Field-specific reporting

Please select the one below that is the best fit for your research. If you are not sure, read the appropriate sections before making your selection.

☒ Life sciences ☐ Behavioural & social sciences ☐ Ecological, evolutionary & environmental sciences

For a reference copy of the document with all sections, see nature.com/documents/nr-reporting-summary-flat.pdf

Life sciences study design

All studies must disclose on these points even when the disclosure is negative.

Sample size	No statistical methods were used to pre-determine samples sizes but our sample sizes are similar to those reported in previous publications: Holz et al. Sci Immunol 5, (2020) and Fernandez-Ruiz et al. Immunity 45, 889–902 (2016). Generally, 5 mice were used per group and then experiments repeated 2-3 times and results pooled.
Data exclusions	Data analyzed included outliers unless explained by technical error
Replication	Each experiment was reproduced at least twice to confirm reproducibility. Except for data in Figure 4f, which was a simple dose-finding experiment.
Randomization	Mice were randomly assigned to each group, but were sex and age matched
Blinding	Investigators were not blinded. Experiments were overseen by a lead researcher with full responsibility for all animal manipulations, including exact contents of vaccines/treatments used. Data collection and analysis were therefore not performed blind to the conditions of the experiments.

Reporting for specific materials, systems and methods

We require information from authors about some types of materials, experimental systems and methods used in many studies. Here, indicate whether each material, system or method listed is relevant to your study. If you are not sure if a list item applies to your research, read the appropriate section before selecting a response.

Materials & experimental systems

n/a	Involved in the study
☐	☒ Antibodies
☒	☐ Eukaryotic cell lines
☒	☐ Palaeontology and archaeology
☐	☒ Animals and other organisms
☒	☐ Clinical data
☒	☐ Dual use research of concern
☒	☐ Plants

Methods

n/a	Involved in the study
☒	☐ ChIP-seq
☐	☒ Flow cytometry
☒	☐ MRI-based neuroimaging

Antibodies

Antibodies used

Antigen/Fluorophore	Identifier	Source	Concentration used (ug/mL)
CD19 eFluor 450	Clone 103 , AB_2734905	eBioScience	0.4
CD44 BV750	Clone IM7, AB_2871973	Biolegend	1.66
CD62LPE-Cy7	Clone MEL-14, AB_31310	Biolegend	0.33
KLRG1 APC	Clone 2F1, AB_10641560	Biolegend	0.33
CD8 AF700	Clone 53-6.7, AB_494005	eBioscience	2.5
H-2Kb/OVA257-264 pentamer PE		Prolmmune	1-3 µL/sample
Viability Zombie NIR		Biolegend	1
TCRβ FITC	Clone H57-597, AB_313429	Biolegend	2.5
CD4 AF532	Clone RM4-5, AB_11218891	Invitrogen	0.22
CD49a B8700	Clone Ha3118, AB_2861198	BD Optibuild	0.33
PD-1 PerCP-eFluor710	Clone RMP1-30, AB_11151142	eBioscience	2
CD103 PE-Dazzle594	Clone 2E7, AB_2566492	Biolegend	2
CD69 PE-Cy5	Clone H1.2F3, AB_313112	Biolegend	0.67
CD101 PE-Cy7	Clone Moushi101, AB_2573378	Invitrogen	0.33
KLRG1 APC	Clone 2F1, AB_10641560	Biolegend	0.33
CD64 AF647	Clone X54-5/7.l, AB_2566561	Biolegend	1.67
CD62L AF700	Clone MEL-14, AB_493719	Biolegend	1.67
CD45.2 APC-Fire750	Clone 104, AB_2629723	Biolegend	0.67
CDld/PBS-57 tetramer BV421		NIH tetramer core facility	1 in 300 dilution
Ly6C APC	Clone AL-21, AB_l727554	BD	0.1
CD19 PerCPCy5.5	Clone ID3/CD19, AB_2629815	Biolegend	0.1
CD8 BV711	Clone 53-6.7, AB_2562100	Biolegend	0.1
NK1.1 PECy7	Clone PK136, AB_394507	BD	0.1
NK1.1 FITC	Clone PK136, AB_39467	BD	0.25
CXCR6 BV421	Clone SA051D1, AB_2616760	Biolegend	0.1
CXCR6 APC	Clone SA051D1, AB_2572143	Biolegend	0.1
Ly6C FITC	Clone HK1.4, AB_1186135	Biolegend	0.05
Ly6G V450	Clone 1A8, AB_1727564	BD	0.1
CD4 FITC	Clone GK1.5, AB_395013	BD	0.15
CX3CR1 BV785	Clone SA011F11, AB_2565938	Biolegend	0.2
CX3CR1 APC	Clone SA011F11, AB_2564492	Biolegend	0.1
PD-l PE-Cy7	Clone 29F.1A12, AB_10689635	Biolegend	0.1
CD62L PerCPCy5.5	Clone MEL-14, AB_2285839	Biolegend	0.1
CD62L BV605	Clone MEL-14, AB_2563058	Biolegend	0.1
CD44 AF700	Clone IM7, AB_493713	Biolegend	0.25
TCRβ APC-Cy7	Clone H57-597, AB_893624	Biolegend	0.2
CD69 PE-Cy5	Clone H1.2F3, AB_468772	eBioscience	0.25
CD45.1 PE-Cy7	Clone A20, AB_1727488	BD	0.05
CD45.2 FITC	Clone 104, AB_313443	Biolegend	0.25
CDld/PBS-44 tetramer BV421, PE		In house	1 in 400 dilution
H-2Kb/ RPL6120-127 tetramer PE		In house	1 in 300 dilution
CD45 BUV395	Clone 30-F11, AB_2651134	BD	0.1
CD3PerCPCy5.5	Clone 17A2, AB_1595492	Biolegend	0.1
CD11c PECy7	Clone N418, AB_493568	Biolegend	0.1
Ly6C APCCy7	Clone HK1.4, AB_10640120	Biolegend	0.1
MHC Class II AF700	Clone M5/114.15.2, AB_494009	eBioscience	0.2
F4/80 BV421	Clone BMS, AB_11203717	Biolegend	0.1
CD11b BV650	Clone Ml/70, AB_2566568	Biolegend	0.2
XCR1 BV785	Clone ZET, AB_2783119	Biolegend	0.2
CD40 PECy5	Clone 3/23, AB_2075922	Biolegend	0.1
CD80 BUV661	Clone 16-1OA1, AB_2870964	BD	0.1
CD86 PE	Clone 24F, AB_394180	BD	0.1
CD70 APC	Clone FR70, AB_2738336	BD	0.1
PD-L1 AF488	Clone MIH5, AB_2811871	eBioscience	0.2
CD19 BUV395	Clone 103, AB_2925256	eBioscience	1.0
CD11b BUV737	Clone Ml/70, AB_2895933	eBioScience	0.2
CD80 BV421	Clone 16-10A1, AB_10900989	Biolegend	0.25
MHC Class II eF450	Clone M5/114.15.2, AB_1272204	eBioScience	0.2
XCR1 BV650	Clone ZET, AB_2566410	Biolegend	1.0
SIRPa BV711	Clone P84, AB_2740429	BD	1.0
CD11c BV786	Clone HL3, AB_2738394	BD	1.0
Siglec-H PerCP-eF710	Clone eBio440C, AB_1834443	eBioScience	1.0
CD40 PE	Clone 3/23, AB_2539239	Invitrogen	0.5
PD-Ll PE-Dazzle594	Clone 10F.9G2, AB_2565638	BioLegend	1.0
CD64 AF647	Clone X54-5/7.1, AB_2566560	BioLegend	1.6
CD86 APC-R700	Clone GU, AB_2739258	BD	0.3
CD45 BUV395	Clone 30-F11, AB_2651134	BD	0.1

Validation

All antibodies are from commercial sources and have been validated by the vendors. Validation data are available on the manufacture's website, summarized below. Antibodies have been titrated by the authors to find the optimal dilution (amount) for staining.

Invitrogen and eBioscience antibodies for flow cytometry from Thermofisher Scientific undergo target validation with a two-part system that includes target specificity verification and functional application validation. Target specificity verification can involve one or more method, examples include but are not limited to target knockout using CRISPR-Cas9 and neutralization using blocking antibodies. Functional application validation assesses performance in the given application (i.e. flow cytometry). https://www.thermofisher.com/nz/en/home/life-science/antibodies/invitrogen-antibody-validation.html. Antibodies are tested with mouse bone marrow cells, splenocytes and/or thymocytes.

Antibodies used for flow cytometry from Biolegend were validated by the supplier for specificity using 1-3 cell lines that are target-positive or -negative using single- or multi-colour flow cytometry analysis. Each new lot of antibody undergoes QC analysis by confirming brightness by MFI compared to the in-date reference lot. https://www.biolegend.com/en-us/quality/quality-control.

BD Biosciences antibodies (including BD OptiBuildTM antibodies) undergo multiple methodologies including flow cytometry, immunofluorescence, immunohistochemistry or western blot on a combination of primary cells, cell lines or transfectant models to confirm specificity. https://www.bdbiosciences.com/en-us/products/reagents/flow-cytometry-reagents/research-reagents/quality-and-reproducibility.

The H-2Kb/OVA257-264 pentamer and H-2Kb/RPL6120-127 tetramer were tested against peptide-specific TCR transgenic T cells (OT-I and PbT-I cells, respectively). The CD1d/PBS-57 tetramer was tested in wild-type and TRAJ18-/- strains for confirmation of staining of type I NKT cells. As well as the CD1d/PBS-44 tetramer made in-house, an unloaded tetramer control was tested beside the PBS-57-loaded tetramer to ensure specific staining with low background, as in Fig. 3 . https://doi.org/10.4049/jimmunol.167.3.1164

Animals and other research organisms

Policy information about studies involving animals; ARRIVE guidelines recommended for reporting animal research, and Sex and Gender in Research

Laboratory animals	Mouse strains used were Swiss Webster, C57BL/6J, Traj18-/-, CD40-/-, Batf3-/-, IAE-/-, IL-15-/- and OT-I. Experiments were performed on mice aged between 6 and 12 weeks of age. Adult Anopheles stephensi mosquitoes strain STE2/MRA-128.
Wild animals	This study did not involve the use of wild animals
Reporting on sex	Mice were sex matched for experiments
Field-collected samples	This study did not involve field collected animals
Ethics oversight	The protocols were approved by the Melbourne Health Research Animal Ethics Committee, University of Melbourne (ethics protocol IDs: 1714302, 1914923) or by the Victoria University of Wellington Animal Ethics Committee (AEC23784 and AEC26384).

Note that full information on the approval of the study protocol must also be provided in the manuscript.

Flow Cytometry

Plots

Confirm that:

☒ The axis labels state the marker and fluorochrome used (e.g. CD4-FITC).

☒ The axis scales are clearly visible. Include numbers along axes only for bottom left plot of group (a 'group' is an analysis of identical markers).

☒ All plots are contour plots with outliers or pseudocolor plots.

☒ A numerical value for number of cells or percentage (with statistics) is provided.

Methodology

Sample preparation

Blood was either collected from the tail veins of mice in tubes containing 10 U heparin (Fig. 1) or collected from the submandibular vein punctured with a 4 nm Goldenrod Animal Lancet and collected into 200 µL of 10 mM EDTA/PBS (Figure 2). Tubes were centrifuged at 1503 x g for 4 min and cells resuspended in 1 mL of RBC lysis solution (QIAGEN). After 20 min at 37 °C leucocytes were harvested by centrifugation and resuspended in 200 µL of FACs buffer (PBS with 5 mM EDTA, 2.5 % BSA) for antibody staining in a 96-well plate.

Livers were collected into tubes containing RPMI, 2 % FCS and 10 U heparin. Each liver was teased through a 70µm cell strainer, washed with RPMI, and the cell suspension resuspended in 30 mL of 35% Percoll (GE Health care) before centrifugation at 500 x g for 20 min at 20-22 °C, with no brake. The cell pellet was incubated in 5 mL RBC lysis solution for 5 min at 20-22 °C, before being washed with 30 mL RPMI and resuspended in 1 mL of FACS buffer for flow cytometry. One fifth of the cell suspension was used for antibody staining. Spleen lymphocytes were isolated by teasing tissue through a 70 µm strainer, washing in RPMI, 2 % FCS, incubating cells in RBC lysis solution for 1-2 min at 20-22 °C, washing again and resuspending in 5 mL FACS buffer. Approximately 1/25th of final volume was used for antibody staining. Lung tissue was incubated for 45 min at 37 °C in 0.1 mg/mL Liberase TL (Roche) 0.2 mg/mL DNAse I (Roche) in 1 mL RPMI before 50 µL of

EDTA (0.5 M solution) was added for a further 5 min. Each lung sample was passed through a 3 mL syringe, teased through 70 µm mesh, incubated in 2 mL RBC lysis solution for 10 min at 20-22 °C, and resuspended in 1 mL FACS buffer: 1/10th of final volume was used for antibody staining.

For the assessment of splenic DCs by flow cytometry, spleens were injected at 4-5 points with 0.5 mL IMDM supplemented with 0.3 mg/mL Liberase TL and 0.2 mg/mL DNAse 1, digested in this mix for 30 min at 37 ºC and then mechanically dissociated through a 70 µm sieve with 20 mL of IMDM. Samples were centrifuged at 572 x g for 4 min, supernatants were discarded, and pellets were resuspended in 2 mL RBC lysis buffer. Samples were centrifuged, resuspended in 1 mL FACs buffer and 100 µL was transferred to a 96-well plate for staining.

Tissue preparation for assessment of liver DC populations was as previously decribed (Beattie L et al 2013 Cell Host Microbe). Briefly, livers were perfused with collagenase type IV (Sigma) and then digested in collagenase for 45 min at 37 oC. Cell suspensions were passed through 70 µm sieves, washed with PBS and resuspended in a 33 % Percoll solution (Sigma). Samples were centrifuged at 693 g for 12 mins, no brake. RBC were removed using lysis buffer and 1/5th isolated cells were stained for flow cytometry analysis.

Instrument

BD LSR Fortessa or Cytek Aurora

Software

BDFACS Diva or Spectroflo

Cell population abundance

OT-I.Ly5.1 cells used for cell transfer experiments (Fig 1, 2, 3 and 8) were counted, and their purity was analyzed by staining with anti-CD8a and anti-Va2 TCR antibodies. For Fig 2. the proportion of naive (CD8+CD44loCD62Lhi) CD8 T cells (OT-I cells) was established by flow cytometry.

Gating strategy

For all analyses cells were gated on using FSC x SSC for lymphocytes, singlet discrimination gates (SSC-A vs SSC-H and/or FSC-A vs SSC-A) and live cells (propidium iodide negative or Viability Zombie NIR negative). In figure 1,2, 3 and 8, donor OT-I.Ly5.1 cells were then selected by gating on CD45.1+ cells followed by cells expressing the activation/memory marker CD44. Memory subsets were delineated using antibodies against CD69 and CD62L. For Figure 2, prior to selecting NKT cells using PBS-57 loaded CD1d tetramers, B cells and macrophages and OT-I.CD45.1 cells were removed from the analysis using antibodies specific for CD45.1, CD19 and CD64. For Figure 4, CD8+ Kb-OVA257-264-specific cells were assessed after removing cells binding to CD64, CD19 and PBS-57 loaded CD1d tetramers, and gating on cells expressing CD45.2, TCRβ and CD44. Memory subsets of CD8+ OVA257-264-specific T cell were delineated using antibodies to CD69 and CD62L. For Figure 5, 6 and 7, B cells were excluded by selecting CD19 negative cells and NKT cells were excluded using PBS-44 loaded CD1d tetramers. Kb-RPL6120-127 tetramer+ cells were analysed by selecting on CD8+ tetramer+ cells and memory subsets were delineated using antibodies against CD69 and CD62L.
To assess splenic dendritic cells in Figure 3, CD45.2+ cells were gated and then selected for lack of expression of CD64 and CD19 before gating on cells expressing MHC II and CD11c. Expression of XCR1 and lack of expression of SIRPα identified as cDC1. For liver dendritic cells, CD45+ cells were selected before removal of Ly6C and F4/80+ populations. Liver dendritic cells were selected by gating on CDllc+/MHC Class II+ cells.

☒ Tick this box to confirm that a figure exemplifying the gating strategy is provided in the Supplementary Information.